

On the topological content of $SU(2)$ gauge fields below T_c

E.-M. Ilgenfritz^a, B. V. Martemyanov^b, M. Müller-Preussker^c,
S. Shcheredin^c and A. I. Veselov^b

^a Research Center for Nuclear Physics, Osaka University, Osaka 567-0047, Japan

^b Institute for Theoretical and Experimental Physics, Moscow 117259, Russia

^c Humboldt-Universität zu Berlin, Institut für Physik, D-10115 Berlin, Germany

October 29, 2018

Abstract

Finite temperature Euclidean $SU(2)$ lattice gauge fields generated in the confinement phase close to the deconfinement phase transition are subjected to cooling. The aim is to identify long-living, almost-classical local excitations which carry (generically non-integer) topological charge. Two kinds of spatial boundary conditions (fixed holonomy and standard periodic boundary conditions) are applied. For the lowest-action almost-classical configurations we find that their relative probability semi-quantitatively agrees for both types of boundary conditions. We find calorons with unit topological charge as well as (anti-)selfdual lumps (BPS-monopoles or dyons) combined in pairs of non-integer (equal or opposite sign) topological charge. For calorons and separated pairs of equal-sign dyons obtained by cooling we have found that (i) the gluon field is well-described by Kraan-van Baal solutions of the Euclidean Yang-Mills field equations and (ii) the lowest Wilson-fermion modes are well-described by analytic solutions of the corresponding Dirac equation. For metastable configurations found at higher action, the multi-center structure can be interpreted in terms of dyons and antidyons, using the gluonic and fermionic indicators as in the dyon-pair case. Additionally, the Abelian monopole structure and field strength correlators between the centers are useful to analyse the configurations in terms of dyonic constituents. We argue that a semi-classical approximation of the non-zero temperature path integral should be built on superpositions of solutions with non-trivial holonomy.

1 Introduction

It is widely accepted that quark confinement in QCD is related to some complex structure of the gauge field vacuum. A popular scenario views the vacuum state as a dual superconductor [1] in four dimensions which is unable to sustain strong gluon electric fields such that flux tubes are formed due to a dual Meissner effect. The analogon to the Cooper pairs of usual superconductors are Abelian monopoles, in other words, condensed magnetic currents belonging to an Abelian subgroup of the strong gauge group.

The lattice evidence in support of this mechanism rests either on the ability to localize the magnetic currents [2, 3] as the worldlines of magnetic defects with respect to some gauge fixing prescription [4], or on the construction of a corresponding monopole creation operator [5] in order to study its condensation. The question how their condensation leads to confinement is relatively well-understood [6, 7], and while also the question of universality with respect to the gauge condition is partly answered affirmatively [8, 9], the reason *why* these monopoles are created in the QCD vacuum is far from being understood.

There is another working picture of the Yang-Mills vacuum [10, 11, 12, 13] which has been applied very successfully to hadron physics, including basic features like chiral symmetry breaking and the $U_A(1)$ anomaly as well as details of spectroscopy [14]. It is based on the instanton, a solution [15] of the Euclidean field equations. However, even in the form of the instanton liquid model [16], when some local interaction between instantons is taken into account, instantons cannot be brought into relation with the third basic feature of QCD, confinement. There have been attempts to stretch the instanton liquid model to its limits in order to provide a confining string tension of sufficient strength between a static quark and antiquark [17], at least at intermediate distances of a few instanton radii. A recent assessment of the instanton-generated forces between static charges has been discussed in Ref. [18].

In lack of a satisfactory instanton-based mechanism of confinement, many indications have been presented that instantons (or, more generally, carriers of topological charge) are closely related to the Abelian monopoles which are usually detected by gauge fixing procedures. This evidence stems from the observation made for one-instanton and many-instanton configurations [19, 20] in the maximally Abelian gauge and from the observation of short range correlations between topological charge and magnetic currents in genuine confining lattice configurations [21, 22]. On the other hand, also in artificial instanton liquid model ensembles (multi(anti)instanton configurations) monopole network percolation has been observed [23] as a prerequisite of monopole condensation. This has led to the conclusion that semi-classical, smooth gauge field configurations can give rise to networks of (light, condensed) magnetic monopoles even if these become discovered only as defects of the gauge fixing process. Thus, some reconciliation of the two pictures seems possible.

However, as long as the instantons are uncorrelated, the Abelian monopoles and center vortices [24] revealed by the respective gauge fixing are quantitatively insufficient to provide confinement [18]. Moreover, the approximate Casimir scaling at intermediate distance that the strong force acting on charges of different representations obeys is also strongly broken in the instanton liquid ensemble [18]. This makes it less likely that in-

stantons are related to confinement even if some important correlation would be included into the model.

Nowadays, in a fresh attempt to relate instanton physics to the confinement property of the Yang-Mills vacuum, instantons dissociated into meron pairs have been investigated with respect to their monopole and center vortex content [25]. Our present work, which also aims to extend the instanton picture, starts from a somewhat different corner, finite temperature. All the criticism with respect to an instanton mechanism of confinement applies also to finite temperature Yang-Mills theory below the deconfinement temperature, where periodic instantons (calorons) are the ingredients of the instanton liquid model [26]. More precisely, there are periodic instantons *with trivial holonomy* which are thought of being the bricks of topological structure. An isolated caloron with trivial holonomy is a periodic classical solution of the Euclidean equations of motion with trivial asymptotics of the Polyakov loop at infinity, $P(\vec{x} \rightarrow \infty) = z \in Z(N)$. These are the "old" calorons first considered by Harrington and Shepard [27].

During the last years new caloron solutions have been found and studied by Kraan and van Baal (KvB) [28, 29] which correspond to a non-trivial asymptotic holonomy $P(\vec{x} \rightarrow \infty) \notin Z(N)$. From our point of view, a particularly interesting feature is that, in the generic case, these configurations are composites of BPS-monopoles [30] (or dyons) *i. e.* lumps carrying non-integer topological charge. A semi-classical description of the (finite temperature) vacuum in the confinement phase, based on these new calorons still remains to be developed. Some new perspectives have been pointed out in Ref. [31]. In the present paper we investigate metastable configurations which appear in the process of cooling [32] in the region of few times the instanton action. These are excitations which might become the building blocks of such a semi-classical description. The topological content, which appears at this deep, almost classical level of cooling, is itself characteristic for the phase (confining or deconfined) where the configurations are taken from before they are cooled. Still, we do not claim that the number and size of topological lumps obtained in this way immediately characterizes the finite-temperature vacuum.

The outcome of cooling with normal periodic boundary conditions has been compared with that of cooling with spatial boundary conditions of prescribed holonomy, which is enforced by cold boundary links appropriately chosen. As for the confinement phase, the dependence on the boundary conditions is weak. A closer check shows that, after cooling with periodic boundary conditions, the average Polyakov loop over regions of low action and topological density is not restricted to trivial holonomy. In other words, in the confined phase non-trivial holonomy boundary conditions for topological charge lumps are provided by the dynamics itself. They do not need to be enforced. In the confined phase these are the natural fluctuating asymptotic conditions for the semi-classical excitations.

Similarly to the studies of the monopole and vortex content of meron [25] pairs, we study here also the monopole content and other signatures of the simplest of these configurations (to be interpreted as dyon-dyon and dyon-antidyon pairs) as potential semi-classical building blocks of a confining vacuum. Preliminary results have been presented in [33, 34, 35].

In contrast to the meron studies [25], instead of tailoring particular semi-classical

configurations, in the present work we are going to demonstrate the emergence under cooling of metastable lattice configurations with low action which (distinguished by action plateaus) resemble the new calorons (dyon-dyon pairs). In this case, where an analytical solution is available, we show that action density, topological density and the profile of the fermionic zero modes on the lattice can be fit simultaneously with the corresponding expressions for the new caloron KvB solution [28, 36]. It is worth noticing that at actions around one instanton action also configurations pop up under cooling which resemble dyon-antidyon pairs. This interpretation is suggested by action and topological density and is corroborated by the zero modes of the Wilson fermion matrix and the Polyakov loop profile. Lacking an analytical solution for these configurations of mixed (anti)selfduality it is impossible to present a fit of the various distributions.

Also for higher metastable plateaus with an action of few times the instanton action a multi-center structure of few-lump dyon-antidyon mixed configurations can be recognized having a broad distribution of holonomy away from the lumps of action and topological charge. We do not claim that this directly proves that the finite temperature vacuum is composed exactly as that gas of dyons and antidyons. Nevertheless, it is remarkable that cooling starting from genuine Monte Carlo configurations in the *deconfined* phase ends in completely different low-action configurations as it has been already claimed in an early related work by Laursen and Schierholz [37].

The paper is organized as follows.

In Section 2 we will collect some necessary formulae covering the zero-temperature instanton, the well-known selfdual finite temperature instanton (the "old caloron"), the new KvB calorons, monopoles as instanton chains etc. This will be needed for the fit of dyon-dyon pairs becoming visible on the lattice.

Section 3 provides all necessary lattice definitions, in particular the boundary conditions and the observables considered in order to identify KvB and other solutions.

In Section 4 we describe the results of a first part of our simulations where equilibrium configurations are cooled down to an action near to the one-instanton action. Although we cool to this low level of action, we find the topological content (and the dependence on the boundary conditions) very different, depending on whether the original Monte Carlo ensemble was describing the confinement or deconfinement phase.

In Section 5 we report on a second part of our study, where higher lying action plateaus, appearing in the process of cooling with periodic boundary conditions, are identified with respect to their dyon content.

Section 6 presents the conclusions.

2 Calorons with trivial and non-trivial holonomy in continuum $SU(2)$ Yang-Mills theory

Throughout this paper $SU(2)$ gauge theory in four-dimensional Euclidean space is considered. We start the description of caloron solutions with generically non-trivial holonomy with the well-known one-instanton solution [15, 38]. In the singular gauge its gauge

potentials are given by

$$A_\mu(x) = \frac{\tau_a}{2} \bar{\eta}_{\mu\nu}^a \partial_\nu \log \phi(x), \quad \phi(x) = 1 + \frac{\rho^2}{(x - x_0)^2}, \quad \mu, \nu = 1, \dots, 4 \quad (1)$$

where $\bar{\eta}_{\mu\nu}^a$ is the 't Hooft tensor, $\tau_a/2$ - denote the generators of the $SU(2)$ group, ρ, x_0 are the size of the instanton and the $4D$ position of its center. For further use we introduce the following notations

$$\begin{aligned} \phi(x) &= \frac{\psi(x)}{\hat{\psi}(x)}, \\ \psi(x) &= 2\pi^2((x - x_0)^2 + \rho^2), \quad \hat{\psi}(x) = 2\pi^2(x - x_0)^2, \\ \chi(x) &= 1 - \frac{1}{\phi} = \frac{2\pi^2\rho^2}{\psi} \end{aligned} \quad (2)$$

and rewrite the instanton fields in the form

$$\begin{aligned} A_\mu(x) &= \frac{1}{2} \bar{\eta}_{\mu\nu}^3 \tau_3 \partial_\nu \log \phi(x) \\ &+ \frac{1}{2} \phi(x) \text{Re}((\bar{\eta}_{\mu\nu}^1 - i\bar{\eta}_{\mu\nu}^2)(\tau_1 + i\tau_2) \partial_\nu \chi(x)). \end{aligned} \quad (3)$$

The next step is to construct the time-periodic instanton or caloron [27]. For this purpose we generalize the function ϕ in Eq. (1)

$$\begin{aligned} \phi(x) &= 1 + \sum_{n=-\infty}^{n=\infty} \frac{\rho^2}{((\vec{x} - \vec{x}_0)^2 + (t - nb)^2)} \\ &= 1 + \frac{\pi\rho^2}{br} \frac{\sinh(\frac{2\pi r}{b})}{\cosh(\frac{2\pi r}{b}) - \cos(\frac{2\pi t}{b})}, \end{aligned} \quad (4)$$

where $r = |\vec{x} - \vec{x}_0|$ and $t = x_4 - x_4^{(0)}$. b is the time period of the periodic instanton solution. For simplicity, $b = 1$ is assumed in the following. Physically, the periodicity b has to be identified with the inverse temperature T^{-1} . Then the caloron potentials are given by Eq. (3) with

$$\begin{aligned} \phi(x) &= \frac{\psi(x)}{\hat{\psi}(x)}, \\ \psi(x) &= \cosh(2\pi r) - \cos(2\pi t) + \frac{\pi\rho^2}{r} \sinh(2\pi r), \quad \hat{\psi}(x) = \cosh(2\pi r) - \cos(2\pi t), \\ \chi(x) &= 1 - \frac{1}{\phi} = \frac{\pi\rho^2 \sinh(2\pi r)}{\psi r}. \end{aligned} \quad (5)$$

This solution can be viewed as a chain of instantons aligned along the temporal direction, separated by distance b but with the same orientation in color space. In the limit $\rho \rightarrow \infty$

it can be transformed into a static solution by an appropriate gauge transformation. This static object can be identified with a BPS monopole [30] in Euclidean space, where the fourth component A_4 plays the rôle of the Higgs field in the adjoint representation. The solution has both electric and magnetic charge. Therefore, we call it also *dyon* (D).

Constructing a caloron with nontrivial holonomy [28] is the next step. It can be approximately viewed as an instanton chain with periodicity b , too, where each of the instantons is rotated with respect to the previous one by an angle $4\pi\omega$ in color space, ω being the parameter of holonomy as we will see below. The rotation axis can be any, for definiteness let us take the third one. The words *approximately viewed* mean that when the instantons are well separated ($\rho/b \ll 1$) the fields near the instanton centers look approximately as described above. The caloron field with nontrivial holonomy is described again by Eq. (3) but now with [28]

$$\begin{aligned}
\phi(x) &= \frac{\psi(x)}{\hat{\psi}(x)}, \\
\psi(x) &= -\cos(2\pi t) + \cosh(4\pi r\bar{\omega}) \cosh(4\pi s\omega) + \frac{(r^2 + s^2 + \pi^2 \rho^4)}{2rs} \sinh(4\pi r\bar{\omega}) \sinh(4\pi s\omega) \\
&\quad + \pi \rho^2 (s^{-1} \sinh(4\pi s\omega) \cosh(4\pi r\bar{\omega}) + r^{-1} \sinh(4\pi r\bar{\omega}) \cosh(4\pi s\omega)), \quad (6) \\
\hat{\psi}(x) &= -\cos(2\pi t) + \cosh(4\pi r\bar{\omega}) \cosh(4\pi s\omega) + \frac{(r^2 + s^2 - \pi^2 \rho^4)}{2rs} \sinh(4\pi r\bar{\omega}) \sinh(4\pi s\omega), \\
\chi(x) &= e^{4\pi i t \omega} \frac{\pi \rho^2}{\psi} \{e^{-2\pi i t} s^{-1} \sinh(4\pi s\omega) + r^{-1} \sinh(4\pi r\bar{\omega})\}
\end{aligned}$$

instead of Eq. (5). The holonomy parameters ω and $\bar{\omega}$ are related to each other as $\bar{\omega} = 1/2 - \omega$, $0 \leq \omega \leq 1/2$. $r = |\vec{x} - \vec{x}_1|$ and $s = |\vec{x} - \vec{x}_2|$ are the 3D distances to the locations of the two centers of the new caloron solution, $\pi \rho^2/b = d \equiv |\vec{x}_1 - \vec{x}_2|$ is expressed by the distance between the centers. From Eqs. (6) it can be easily seen that, when $\omega \rightarrow 0$ or $\bar{\omega} \rightarrow 0$, the caloron with nontrivial holonomy turns into the Harrington-Shepard caloron described by Eqs. (5). When the separation between the centers becomes large, $d = \pi \rho^2/b \gg 1$, two well-separated constituents emerge which are static in time. The "mass" ratio of these dissociated constituents is equal to $\bar{\omega}/\omega$. Since the full solution is selfdual, the ratio is the same for the action as for the equal-sign topological charge carried by the constituents, the latter summing up to one unit of topological charge, $Q_t = 1$. The separated constituents form a pair of BPS monopoles (or dyons) with opposite magnetic charges. In the following we will call it a DD pair, while non-dissociated calorons will be denoted as CAL , although all these objects represent limiting cases of one and the same solution. The single dyon originally obtained from the Harrington-Shepard caloron in the infinite size limit $\rho \rightarrow \infty$ can be recovered from the new solution by sending the mass of the second constituent to zero and simultaneously its position to spatial infinity.

The action density in all three cases described above can be expressed by a simple formula

$$s(x) = -\frac{1}{2} \partial_\mu^2 \partial_\nu^2 \log \psi(x). \quad (7)$$

So far, the new caloron solution is in the so-called algebraic gauge [29]. It can be made periodic by a gauge transformation which is non-periodic in time $g(x) = e^{-2\pi i t \omega \cdot \tau_3}$,

$$A_\mu^{\text{per}} = \frac{1}{2} \bar{\eta}_{\mu\nu}^3 \tau_3 \partial_\nu \log \phi + \frac{1}{2} \phi \operatorname{Re} \left((\bar{\eta}_{\mu\nu}^1 - i \bar{\eta}_{\mu\nu}^2) (\tau_1 + i \tau_2) (\partial_\nu + 4\pi i \omega \delta_{\nu,4}) \tilde{\chi} \right) + \delta_{\mu,4} 2\pi \omega \tau_3, \quad (8)$$

where

$$\tilde{\chi} \equiv e^{-4\pi i t \omega} \chi = \frac{\pi \rho^2}{\psi} \left\{ e^{-2\pi i t} s^{-1} \sinh(4\pi s \omega) + r^{-1} \sinh(4\pi r \bar{\omega}) \right\}. \quad (9)$$

Now the time component of the caloron potential has become nonzero at spatial infinity. We can define the *holonomy* which becomes non-trivial

$$\mathcal{P}(\vec{x}) = \text{P exp} \left(i \int_0^b A_4(\vec{x}, t) dt \right) \rightarrow \mathcal{P}_\infty = e^{2\pi i \omega \tau_3} \quad \text{for } |\vec{x}| \rightarrow \infty. \quad (10)$$

In terms of ω , the normalized trace of the holonomy, the Polyakov loop which we shall take as a direct *measure of the holonomy*, at spatial infinity becomes

$$L(\vec{x}) \equiv \frac{1}{2} \operatorname{tr} \mathcal{P}(\vec{x}) \rightarrow L_\infty \equiv \frac{1}{2} \operatorname{tr} \mathcal{P}_\infty = \cos(2\pi \omega). \quad (11)$$

In the special case $\omega = \bar{\omega} = 1/4$ the measure of holonomy is equal to zero and the two constituent dyons acquire equal mass, *i. e.* equal action and topological charge. For our later purposes it is useful to remember that the Polyakov loop has peaks $L(\vec{x}) = \pm 1$ very close to the center positions $\vec{x} = \vec{x}_{1,2}$ of the constituents [28].

For well-separated dyons, when the functions $\phi(x)$ and $\psi(x)$ are almost time independent, the strongest time dependence comes from the first part of the function $\tilde{\chi}(x)$. This dependence is represented by the phase $e^{-2\pi i t}$ and is nothing else but the homogeneous rotation of the first dyon, which has $L(\vec{x}_1) = -1$, in color space around the third axis with angle 2π over the period. The second dyon with $L(\vec{x}_2) = +1$ is static. Such a relative rotation of two dyons (that form a monopole-antimonopole pair) gives the so-called *Taubes winding* necessary two produce unit topological charge from a monopole-antimonopole pair [39]. One can detect this rotation in a gauge invariant fashion by looking at the gauge invariant field strength correlator defined on each constant-time slice and watching its evolution over the periodicity interval b . The field strength is selfdual ($E_k^a = B_k^a$ or antiselfdual, $E_k^a = -B_k^a$) everywhere in the KvB caloron. The electric field $E_k^a(\vec{x}_i, t)$ at the centers of both dyons $i = 1, 2$ is proportional to an orthogonal matrix (in both the $SU(2)$ color and space indices). Thus the three ($k = 1, 2, 3$) components $E_k^a(\vec{x}_1)$ of the electric field form vectors in color space which represent a local reference frame at the center of the first dyon. The comparison with the local frame at the center of the other dyon, \vec{x}_2 , can be made in a gauge invariant manner by connecting the centers by the (fixed time) Schwinger line parallel transporter

$$\mathcal{S}(\vec{x}_1, t; \vec{x}_2, t) = \text{P exp} \left(i \int_{\vec{x}_2}^{\vec{x}_1} A_k^a(\vec{x}', t) \frac{\vec{\tau}^a}{2} dx'_k \right). \quad (12)$$

Using this one can form the gauge invariant field strength product

$$R_{kl}^{12}(t) = \text{tr} \left(E_k(\vec{x}_1, t) S(\vec{x}_1, t; \vec{x}_2, t) E_l(\vec{x}_2, t) S^+(\vec{x}_1, t; \vec{x}_2, t) \right) \quad (13)$$

which is again an orthogonal matrix. This matrix performs a full rotation with the Euclidean time t running from 0 to b .

Finally, let us comment on the zero-mode eigenfunctions of the fermionic massless Dirac operator in the background of the KvB solutions. They have been studied analytically in [40] and [36]. One finds closed solutions depending on the type of (anti)periodic boundary conditions (b.c.) imposed on the fermion fields in the imaginary time direction. In case of well-separated dyon pairs, *i. e.* for $d = \pi\rho^2/b \gg 1$, the zero eigenmode densities become very simple expressions

$$\begin{aligned} |\psi^-(x)|^2 &= -\frac{1}{4\pi} \partial_\mu^2 [\tanh(2\pi r \bar{\omega})/r] && \text{for antiperiodic b.c. ,} \\ |\psi^+(x)|^2 &= -\frac{1}{4\pi} \partial_\mu^2 [\tanh(2\pi s \omega)/s] && \text{for periodic b.c. .} \end{aligned} \quad (14)$$

This means that the zero-mode eigenfunctions are localized always around one of the constituents of the KvB solution, for antiperiodic b. c. at that constituent which has $L(\vec{x}) = -1$ at its center \vec{x}_1 . Switching to periodic b.c. for the fermion fields the zero mode localization jumps to the other constituent monopole of the gauge field. Therefore, the fermionic zero modes provide a convenient way to identify a monopole-pair structure in the gauge fields.

3 Detecting dyons and calorons on the lattice

Our first aim was to detect the simplest dyon configurations in the context of finite temperature lattice simulations. For this purpose we have considered $SU(2)$ lattice gauge theory on an asymmetric lattice using the standard Wilson plaquette action with coupling $\beta = 4/g_0^2$,

$$\begin{aligned} S &= \sum_{\vec{x}, t} s(\vec{x}, t) = \sum_{\vec{x}, t} \sum_{\mu < \nu} s(\vec{x}, t; \mu, \nu), \\ s(\vec{x}, t; \mu, \nu) &= \beta \left(1 - \frac{1}{2} \text{tr} U_{x, \mu\nu} \right), \quad U_{x, \mu\nu} = U_{x, \mu} U_{x+\hat{\mu}, \nu} U_{x+\hat{\nu}, \mu}^\dagger U_{x, \nu}^\dagger \end{aligned} \quad (15)$$

and periodic boundary conditions in all four (toroidal) directions. For simplicity the lattice spacing is set to $a = 1$. The lattice size will be $N_s^3 \times N_t$ with the spatial extension $N_s = 16$ or 24 and with $T^{-1} \equiv N_t = 4$. For $N_t = 4$ the model is known to undergo the deconfinement phase transition at the critical coupling $\beta_c \simeq 2.299$ [41]. Throughout this paper we concentrate on the confinement phase, *i. e.* $\beta \leq \beta_c$.

We shall generate the quantum gauge field ensemble $\{U_{x, \mu}\}$ by simulating the canonical partition function using the standard heat bath Monte Carlo method. The equilibrium field configurations will be cooled by iteratively minimizing the action S . Usually, cooling

in one or another form is used in order to smooth out short-range fluctuations, while (initially) leaving some long-range physics intact. The cooling method applied here is the standard relaxation method described long time ago in [32].

This method, if applied without any further limitation, easily finds approximate solutions of the lattice field equations as shoulders (plateaus) of action in the relaxation history. Under certain circumstances, this defines and preserves the total topological charge of a configuration. However, the short-range structure of the vacuum fields is changed. Still, the type of classical solutions, which are being selected, depends on the phase which the quantum ensemble $\{U_{x,\mu}\}$ is meant to describe. We want to investigate smoothed fields at different stages of cooling, by using a stopping criterium which selects the plateaus in a given interval of action. First, in Sect. 4, we focus at the lowest action plateaus, i.e. $S = (0.5 \cdots 1.5) S_{\text{inst}}$, where $S_{\text{inst}} = 8\pi^2/g_0^2$ denotes the action of a continuum instanton. Lateron, in Sect. 5, we shall describe more complex approximate solutions found by stopping at higher plateaus.

The smoothed fields will be analyzed according to the spatial distributions of the following observables:

- *action density* computed from the local plaquette values and averaged with respect to the time variable:

$$\varsigma(\vec{x}) = \frac{1}{N_t} \sum_t s(\vec{x}, t); \quad (16)$$

- *topological density* computed with the standard discretization and averaged over the time variable:

$$q_t(\vec{x}) = -\frac{1}{N_t} \frac{1}{2^4 \cdot 32\pi^2} \sum_t \left(\sum_{\mu,\nu,\rho,\sigma=\pm 1}^{\pm 4} \epsilon_{\mu\nu\rho\sigma} \text{tr} [U_{x,\mu\nu} U_{x,\rho\sigma}] \right); \quad (17)$$

- *Polyakov loop* defined as:

$$L(\vec{x}) = \frac{1}{2} \text{tr} \prod_{t=1}^{N_t} U_{\vec{x},t,4}, \quad (18)$$

where the $U_{\vec{x},t,4}$ represent the links in time direction;

- *Abelian magnetic fluxes and monopole charges* defined within the maximally Abelian gauge (MAG). The latter is found by maximizing the gauge functional

$$F[g] = \sum_{x,\mu} \text{tr} (U_{x,\mu}^g \tau_3 U_{x,\mu}^{g\dagger} \tau_3), \quad (19)$$

with respect to gauge transformations $U_{x,\mu} \rightarrow U_{x,\mu}^g = g(x) U_{x,\mu} g^\dagger(x + \hat{\mu})$. Abelian link angles $\theta_{x,\mu}$ are then defined by Abelian projection onto the diagonal $U(1)$ part of the link variables $U_{x,\mu} \in SU(2)$. According to the DeGrand-Toussaint prescription [2] a gauge invariant magnetic flux $\bar{\Theta}_p$ through an oriented plaquette $p \equiv (x, \mu\nu)$

is defined by splitting the plaquette $\Theta_p = \theta_{x,\mu} + \theta_{x+\hat{\mu},\nu} - \theta_{x+\hat{\nu},\mu} - \theta_{x,\nu}$ into $\bar{\Theta}_p = \Theta_p + 2\pi n_p$, $n_p = 0, \pm 1, \pm 2$ such that $\bar{\Theta}_p \in (-\pi, +\pi]$. The magnetic charge of an elementary 3-cube c is then $m_c = \frac{1}{2\pi} \sum_{p \in \partial c} \bar{\Theta}_p$;

- *eigenvalues and eigenmode densities* of the non-Hermitian standard Wilson-Dirac operator

$$\sum_{y,s,\beta} D[U]_{xr\alpha,ys\beta} \psi_{s\beta}(y) = \lambda \psi_{r\alpha}(x) \quad (20)$$

with

$$\begin{aligned} D[U]_{xr\alpha,ys\beta} &= \delta_{xy} \delta_{rs} \delta_{\alpha\beta} \\ &- \kappa \sum_{\mu} \left\{ \delta_{x+\hat{\mu},y} (\mathbf{1}_D - \gamma^{\mu})_{rs} (U_{x,\mu})_{\alpha\beta} + \delta_{y+\hat{\mu},x} (\mathbf{1}_D + \gamma^{\mu})_{rs} (U_{y,\mu}^{\dagger})_{\alpha\beta} \right\} \end{aligned}$$

studied both with time-antiperiodic and time-periodic boundary conditions. For our purposes it will be sufficient to consider this operator which breaks explicitly chiral invariance. To use a chirally improved lattice Dirac operator would be a next step. We find the λ spectrum and the eigenfunctions with the help of the implicitly restarted Arnoldi method [42, 43] and use the standard ARPACK code package for this aim.

For production and cooling of the equilibrium gauge field configurations we shall use two kinds of spatial boundary conditions as in [34] and with preliminary results presented in [35]

1. standard periodic boundary conditions (p.b.c) on the $4D$ torus;
2. fixed holonomy boundary conditions (f.h.b.c.): fixed holonomy is realized by cold timelike links $U_{\vec{x},t,4}$ on the spatial boundary Ω .

For clarity we stress, that the second case is periodic, too, but for the spatial boundary

$$\Omega = \{ \vec{x} \mid \vec{x} = (1, x_2, x_3), (x_1, 1, x_3) \text{ or } (x_1, x_2, 1) \}$$

all time-like links $U_{\vec{x},t,4}$ are frozen to constant group elements. For definiteness we have used embedded pure Abelian link variables $U_{\vec{x},t,4} \equiv \cos \theta + i\sigma_3 \sin \theta$. In the confinement phase at $\beta \leq \beta_c$ we require $L(\vec{x}) = 0 = \langle L \rangle$ (corresponding to holonomy parameter $\omega = 1/4$) which is satisfied by $\theta = \pi/2N_t$. As in [34] we have studied also the deconfinement case ($\beta > \beta_c$). In this case we fixed the boundary time-like links such that $L(\vec{x}) = \langle L \rangle$ for $\vec{x} \in \Omega$. In both cases $\langle L \rangle$ denotes the ensemble average $\langle |\sum_{\vec{x}} L(\vec{x})| / N_s^3 \rangle$ of the volume-averaged Polyakov loop.

Each kind of boundary conditions will be employed both for the Monte Carlo production of configurations and for their subsequent cooling.

4 Dyonic lumps and other objects seen on the lattice

In a first part of our investigation we have searched for topologically non-trivial objects with lowest possible action, late in the cooling history, in order to find systematic dependences of the selected solutions on the spatial boundary conditions and on the temperature of the original Monte Carlo ensemble. Cooling was stopped at some (n -th) cooling iteration step when the following criteria for the action S_n were simultaneously fulfilled:

- $S_n < 1.5 S_{\text{inst}}$,
- $|S_n - S_{n-1}| < 0.01 S_{\text{inst}}$,
- $S_n - 2 S_{n-1} + S_{n-2} < 0$.

The last condition means that cooling just passed a point of inflection.

For each $\beta \leq \beta_c$ we have scanned the topological content of $O(200)$ configurations. In this late stage of cooling we find approximate classical solutions which are more or less static in time besides non-static ones.

For both kinds of boundary conditions, among the solutions we have found there are such which can be easily identified as *CAL* and *DD*. In order to allow a simple distinction between the non-static calorons *CAL* and the dissociated but static *DD* pairs we introduce a quantity which represents for an Euclidean configuration the mobility of the action density. For brevity, we call it *non-stationarity*

$$\delta_t = \sum_{t, \vec{x}} \sum_{\mu < \nu} |s(\vec{x}, t; \mu, \nu) - s(\vec{x}, t - 1; \mu, \nu)| / S. \quad (21)$$

The action density per plane $s(\vec{x}, t; \mu, \nu)$ and the normalization factor, the total action S , are defined in (15). We have monitored how frequently objects with given δ_t are found at the lowest action plateaus. The histograms of δ_t look similar for both types of boundary conditions. For $\beta = 2.2$ they have a peak at $\delta_t = 0.02 - 0.04$ and a long tail for large δ_t .

We have convinced ourselves that a cut $\delta_t < 0.17$ well separates *DD*-objects which are static with two well-separated maxima of the densities of the topological charge $q_t(\vec{x})$ and action $\varsigma(\vec{x})$. For $\delta_t > 0.17$ the objects can be easily interpreted as *CAL* which are non-static, with an approximately $O(4)$ rotationally symmetric action distribution, with a single maximum of $q_t(\vec{x})$ and $\varsigma(\vec{x})$ in $3D$ space. Both *DD* and *CAL* are showing a pair of opposite-sign peaks of the Polyakov loop.

4.1 *DD* pairs

For a special *DD* solution found with p.b.c., we show in Figs. 1 (a) and (b) two-dimensional cuts of the topological charge density $q_t(\vec{x})$ (a) and of the Polyakov loop distribution $L(\vec{x})$ (b). The *DD* solution was obtained from an equilibrium configuration representing $\beta = 2.2$, *i. e.* the confinement phase. We clearly see the opposite-sign peaks of the Polyakov loop variable correlated with the equal-sign maxima of the topological

charge density. The boundary values of the Polyakov loop are slightly varying because they are not fixed here to a well-defined value. This is the only difference observed between the two types of boundary conditions. In principle, for p.b.c. the holonomy could be arbitrary. What really happens to the asymptotic holonomy we will discuss in Section 5. As a consequence the ratio of the action carried by the well-separated dyon constituents can take any value.

For the same DD solution, Figs. 1 (c) and (d) show the scatter plot of the 70 lowest complex Wilson fermion eigenvalues (20) for $\kappa = 0.14$, both for time-periodic (c) and time-antiperiodic (d) boundary conditions for the fermion fields. In both cases we find one isolated low-lying real eigenvalue which can be related to a zero-mode of the zero-mass continuum Dirac operator. The corresponding (projected) eigenmode densities $\psi^\dagger\psi(x)$ are drawn below, in Figs. 1 (e) and (f). They show a localization behavior as analytically proposed in Eqs. (14). For the time-antiperiodic b.c. the eigenmode is localized at the dyon exhibiting the negative peak of the Polyakov loop related to Taubes winding [36].

For the given solution created on the lattice we have carried out a fit with the analytic formula [28] to reproduce the action density (7). This has provided the parameter values $\vec{x}_1 = (8, 5, 11)$, $\vec{x}_2 = (5, 8, 5)$ and $\omega = 0.202$. Fig. 2 shows one-dimensional projections of the same gauge field configuration together with the analytical results produced with the given fit parameters for the topological density, the Polyakov loop and the fermionic mode density with time-antiperiodic and -periodic boundary conditions according to the expressions (14). The last two curves are predictions, rather than fits. There is an impressive agreement with the numerical shape of the fermionic zero-mode density.

Gauge fixing to MAG we can search for the Abelian monopole content of the field configurations under inspection. We are interested in the positions of the world lines of monopole-antimonopole pairs. For static DD solutions we always find a pair of static (anti)monopoles with world lines coinciding with the centers of the dyons. All these features have been observed for DD -solutions irrespective of the spatial boundary conditions imposed in the process of cooling.

4.2 CAL configurations

In Fig. 3 we show a typical CAL solution, with an approximately $4D$ rotationally invariant action distribution, obtained at $\beta = 2.2$ from cooling with periodic boundary conditions. The configuration possesses a large value of the non-stationarity δ_t . Again we plot $2D$ cuts for the topological charge density, for the Polyakov loop and the fermionic eigenvalues together with the eigenmode density for the distinct real eigenvalue. The full topological charge Q_t is unity. The expected pair of narrow opposite-sign peaks of the Polyakov loop is nicely visible.

The fermionic zero-modes for time-periodic and time-antiperiodic b.c. for this configuration are only slightly shifted relative to each other. A reasonable fit with the analytic solution can be obtained showing that this caloron is nothing but a limiting case of the generic DD solutions. At that point we may conclude that cooling, even with non-fixed holonomy, yields almost-classical solutions which show all characteristics of the

KvB calorons. The typical *CAL* configurations show, after putting them into MAG, a closed Abelian monopole loop circulating around the maximum of the action density in the $4D$ -space.

4.3 $D\bar{D}$ pairs

As previously observed for the case with f.h.b.c. [34], we have found also other field configurations with an action on the instanton level, $S \simeq S_{\text{inst}}$, which are very stable against cooling which motivates us to interpret them also as approximate solutions of the lattice equations of motion. With very low non-stationarity $\delta_t = 0.004 \pm 0.002$, they consist of two lumps of action with opposite-sign topological charge densities. We call them dyon-antidyon pairs, $D\bar{D}$. Each of their lumps turns out approximately (anti)self-dual. The total topological charge of the entire configuration is always zero. Therefore, each of the lumps carries half-integer topological charge. The Polyakov loop exhibits two peaks, in this case of equal sign.

Also for $D\bar{D}$ pairs MAG fixing offers an Abelian monopole interpretation. After Abelian projection a static Abelian monopole-antimonopole pair can be found at the positions of the topological charge centers.

Searching for the eigenvalues of the Wilson-Dirac operator we did not find real eigenvalues but sometimes pairs of complex conjugated eigenvalues with very small imaginary parts. This feature is very similar to that of dilute superpositions of instantons with antiinstantons. This gives us good reason to interpret $D\bar{D}$ pairs as superpositions of single BPS solutions with half-integer topological charge. To the best of our knowledge, analytic solutions of this kind have not been reported in the literature. An example for a $D\bar{D}$ pair is reproduced in Fig. 4. We did not find any real or near-to-real modes for the time-antiperiodic boundary conditions.

4.4 The composition of the lowest action plateaus

Finally, by cooling with both kinds of spatial boundary conditions we have found objects becoming very stable at even lower action, for lattice size $16^3 \times 4$, $S \simeq S_{\text{inst}}/2$ and $\simeq S_{\text{inst}}/4$. Their (color-) electric contribution to the action is very small compared with the magnetic contribution. Moreover, they are perfectly static with $\delta_t = 0.003 \pm 0.002$. Employing MAG we have convinced ourselves that they are purely Abelian. In the confinement phase they are occurring quite rarely directly in the cooling process. They are more common to appear after monopole-antimonopole pairs observed at $S \approx S_{\text{inst}}$ annihilate in the final stage of the relaxation. Therefore, we shall not consider them in detail here. But they seem to play an important rôle in the deconfinement phase [37, 35]. Since they are purely magnetic solutions - pure magnetic fluxes or 't Hooft-Polyakov-like monopoles - we shall abbreviate them M .

In Table 1 the relative frequencies to find different types of classical configurations (DD , CAL , $D\bar{D}$ and M) at and below the one-instanton action plateaus are shown. We compare here p.b.c. with f.h.b.c. For each $\beta \leq \beta_c$ we have investigated $O(200)$ Monte

Carlo equilibrium configurations. We can conclude that cooling applied to configura-

Table 1: Relative frequencies of the occurrence of different kinds of (approximate) solutions, for different values of β and for both kinds of boundary conditions of the gauge field (f.h.b.c. and standard p.b.c.). The lattice size is $16^3 \times 4$.

Type of solution	Boundary condition	$\beta = 2.20$	$\beta = 2.25$	$\beta = 2.30 \simeq \beta_c$
DD	f.h.b.c.	0.46 ± 0.05	0.52 ± 0.05	0.45 ± 0.05
	p.b.c.	0.43 ± 0.05	0.44 ± 0.05	0.23 ± 0.03
CAL	f.h.b.c.	0.19 ± 0.03	0.17 ± 0.03	0.15 ± 0.03
	p.b.c.	0.24 ± 0.03	0.26 ± 0.03	0.26 ± 0.03
$D\bar{D}$	f.p.b.c.	0.28 ± 0.04	0.26 ± 0.04	0.31 ± 0.04
	p.b.c.	0.18 ± 0.03	0.16 ± 0.03	0.10 ± 0.02
M	f.p.b.c.	0.01 ± 0.01	0.01 ± 0.01	0.03 ± 0.01
	p.b.c.	0.04 ± 0.02	0.03 ± 0.01	0.10 ± 0.02
trivial vacuum	f.p.b.c.	0.06 ± 0.02	0.04 ± 0.02	0.06 ± 0.02
	p.b.c.	0.11 ± 0.02	0.11 ± 0.02	0.31 ± 0.04

tions in the confinement phase produces all objects with relative probabilities which are approximately independent of the type of boundary conditions imposed.

For the deconfinement phase we have seen that the strong enhancement of $D\bar{D}$ configurations earlier found for cooling with f.h.b.c. [34] (which would be compatible with the suppression of the topological susceptibility) is not reproduced under cooling with standard p.b.c. In the standard case, the probability to obtain any topologically non-trivial object drops sharply with $\beta > \beta_c$. Cooling down to the one-instanton action plateaus provides only trivial vacuum or M -configurations. Because this latter observation was based on a physically small 3-volume ($16^3 * 4$ for $\beta = 2.4$) finite-size effects might have been too strong to preclude a final conclusion. The structure of cooled deconfined configurations will be addressed in a further investigation.

The independence of the boundary conditions, however, in the confinement phase has to be taken seriously: the enforcement of a $L = 0$ boundary condition seems to be not far from the situation with standard periodic boundary conditions in the MC equilibrium. Some details will be discussed in the next Section.

5 Dilute gas configurations of dyons and antidyons at higher action plateaus

Within the confinement phase, for $0 < T \leq T_c$ and for both kinds of spatial boundary conditions, we have also studied in detail semi-classical configurations at higher action

plateaus. They represent snapshots of earlier stages of the cooling histories because the stopping criteria were focussed on multiples of the instanton action. This study should allow us to observe superpositions of classical solutions studied in Section 4 promising to be relevant for a semi-classical approximation of the non-zero T partition function. So far in the literature, the semi-classical approach to QCD at non-zero temperature is entirely based on Harrington-Shepard caloron solutions with trivial holonomy [27, 26]. Our main concern is here, whether superpositions of solutions with non-trivial holonomy naturally occur under cooling.

5.1 Landscapes of topological density and Polyakov loop, fermion zero modes and Abelian monopoles as dyon finder

Therefore, we expose equilibrium Monte Carlo lattice gauge field configurations to cooling, this time stopping under criteria which apply to different, subsequent action windows. We have been monitoring the landscape of topological density, of the Polyakov line operator as well as the localization of the fermionic zero-modes in the semiclassical candidate configurations.

Searching for more complex approximate classical solutions we have modified our previous stopping criterion, triggering now on:

- $(m - \frac{1}{2})S_{\text{inst}} < S_n < (m + \frac{1}{2})S_{\text{inst}}, \quad m = 2, 3, \dots, \quad \text{and}$
- $S_n - 2 S_{n-1} + S_{n-2} < 0.$

In particular we inspected the first (highest) visible plateaus which occurred at various m -values, typically in the range $m \simeq 8 \div 20$ for $\beta = 2.2$ on a lattice of the size $16^3 \times 4$. Then, we looked at the series of subsequent action plateaus. In terms of the objects classified in Section 4, we have scanned the resulting plateau configurations.

For more definiteness concerning the moment of taking snapshots of the configurations undergoing cooling along a plateau, we have additionally introduced a measure Δ for the mean violation of the classical lattice field equations per link (see [32])

$$\Delta = \frac{1}{8N_s^3 N_t} \sum_{x,\mu} \left\{ \text{tr} \left[(U_{x,\mu} - \bar{U}_{x,\mu})(U_{x,\mu} - \bar{U}_{x,\mu})^\dagger \right] \right\}^{\frac{1}{2}}, \quad (22)$$

where

$$\bar{U}_{x,\mu} = c \sum_{\nu > \mu} \left[U_{x,\nu} U_{x+\hat{\nu},\mu} U_{x+\hat{\mu},\nu}^\dagger + U_{x-\hat{\nu},\nu}^\dagger U_{x-\hat{\nu},\mu} U_{x+\hat{\mu}-\hat{\nu},\nu} \right] \quad (23)$$

is the local link x, μ being the solution of the lattice equation of motion, with all degrees of freedom coupled to it being fixed. The factor c is just a normalization of the staple sum such that $\bar{U}_{x,\mu} \in SU(2)$ ¹.

On the *first* visible plateau we find a gas of localized lumps carrying topological charge, where an identification in terms of dyons D and/or antidyons \bar{D} is still difficult.

¹The replacement $\bar{U}_{x,\mu} \rightarrow U_{x,\mu}$ is exactly the local cooling step as applied throughout this paper.

Independent of the kind of boundary conditions employed, at somewhat lower action plateaus with $m < 10$, we are able to clearly recognize dyons D and antidyons \bar{D} carrying non-integer topological charges. During cooling more and more of these objects disappear. However, at all plateaus we observe an even number of peaks of the spatial Polyakov loop landscape $|L(\vec{x})|$. For illustration see Figs. 5 – 9, which show one and the same gauge field configuration at different stages of the cooling process. In this case f.h.b.c. have been used.

In Fig. 5 we show the action (in units of the instanton or caloron action), the non-stationarity δ_t , and the mean violation Δ of the lattice field equations per link. At three subsequent, already lower action plateaus (labelled by m) we indicate the iteration steps A (for $m = 4$), B (for $m = 3$) and C (for $m = 2$), respectively, where Δ passes through local minima. The corresponding semi-classical field configurations are then displayed in Fig. 6 by means of the $2D$ -projected (by summing with respect to the third coordinate) spatial topological charge density and the $2D$ projected Polyakov loop distribution. More or less well one can recognize in these Figures that at stage A we have a superposition of 6 dyons and 2 antidyons. The topological charge sector has been independently determined to be $Q_t = 2$. A $D\bar{D}$ pair decays or annihilates from A to B such that we have 5 dyons and 1 antidyon at the next stage. The topological charge did not change. Finally, stage C exhibits a superposition of 4 dyons, again with $Q_t = 2$. The latter configuration is very stable. While it stays at the same action over thousands of cooling sweeps, the non-stationarity δ_t gradually rises. A closer look then shows that the scale size of one of the dyon pairs shrinks, transforming this pair into a small undissociated and non-static caloron, which finally disappears after having turned into a tiny dislocation strongly violating the equations of motion (compare with Fig. 5). The average violation of the equations of motion per link peaks immediately before the configuration drops to the next plateau.

This example shows that we have superpositions of non-integer Q_t lumps, which can be interpreted as described in the previous Section. To make sure that this is really the case we provide also the eigenvalue scatter plots for the Wilson-Dirac operator for stage A (Fig. 7), for stage B (Fig. 8) and for stage C (Fig. 9). Fig. 7 shows four real fermion modes (under time-periodic boundary conditions) which could suggest an interpretation of configuration A as a superposition of 3 DD pairs and a single $\bar{D}\bar{D}$ pair. However, the inspection of the time-antiperiodic b.c. case provides only two real modes which supports a dyonic content consisting of 2 DD pairs plus 2 $\bar{D}\bar{D}$ pairs, an interpretation which naively is possible as well. In the stage C, also for time-periodic boundary conditions, we see clearly two real modes sitting on top of two dyon lumps. We have checked that the modes jump to the remaining dyon lumps when changing the fermionic boundary condition to time-antiperiodic.

We have studied also the Abelian (anti)monopole structure after fixing to the MAG and Abelian projection. We see a strong correlation of the peaks of the Polyakov loop with the positions of the (anti)monopoles. This can be seen in Fig. 10. The pair structure in terms of Abelian monopoles, occurring on all action plateaus and the annihilation of single (monopole-antimonopole) pairs during further relaxation, provides an additional

signal for the topological content as superpositions of non-trivial holonomy CAL , DD ($\bar{D}\bar{D}$) or $D\bar{D}$ pairs.

5.2 The rôle of the boundary conditions: are non-trivial boundary conditions "natural" ?

In order to understand this from the point of view of single caloron solutions with non-trivial holonomy we have to find out whether (approximately) those asymptotic holonomy boundary conditions as typical for the dyonic (antidionic) semi-classical background excitations are actually present during the cooling process when periodic boundary conditions (no particular holonomy boundary conditions !) are applied to the full volume. Then it would be easier to accept that similar (albeit fluctuating) boundary conditions might also be realized in the semi-classical vacuum.

To answer this question we *define* the *asymptotic holonomy* L_∞ of a cooled configuration as the average of $L(\vec{x})$ over all points \vec{x} in $3D$ space for which the $3D$ projected action density satisfies $\varsigma(\vec{x}) \leq .0001$, i.e. it takes minimal values which are typically seen in deep valleys around the topological lumps.

In Fig. 11 we show histograms of L_∞ obtained at different plateaus during the cooling histories of an ensemble of $O(200)$ configurations produced at $\beta = 2.2$ on a $16^3 \times 4$ lattice with standard p.b.c. We see a clear peak at $L_\infty = 0$ for higher action plateaus. The distribution is more narrow, than the pure Haar measure would tell us. However, approaching lower-lying plateaus, the real distribution becomes flat.

Closing the discussion of the local boundary conditions, let us finally concentrate on those configurations which belong to the bins of $-1/6 < L_\infty < +1/6$, i.e. those which realize $L_\infty \approx \langle L \rangle$ in the confined phase. For these configurations we turn our attention to the local correlation between the Polyakov loop $L(\vec{x})$ and the action density values $\varsigma(\vec{x})$ measured at the same positions \vec{x} . We studied *conditional distributions* $P[L|\varsigma]$ of the Polyakov loop values $L(\vec{x})$ at spatial points where the spatial action density $\varsigma(\vec{x})$ equals ς . The distributions are normalized for each bin of ς . The distributions are shown as surface plots in Fig. 12 for different plateaus. They show that with higher action density the corresponding local Polyakov loop values tend to be closer to the peak values $L = \pm 1$. The distributions do not depend on which action plateau they were collected. We have identified in Section 4 KvB solutions and $D\bar{D}$ configurations at the one-instanton action plateau, and we have strong indications that the same objects occur on the higher action plateaus, too, i.e. in superpositions of topologically non-trivial lumps of action. This argument is also supported by a comparison with the same kind of conditional distribution obtained from the analytic KvB solution with random parameter distribution which we have discretized on the lattice. The resulting distribution $P[L|\varsigma]$ is shown in Fig. 13 (a) and compared with the distribution for calorons with trivial holonomy (b).

5.3 The Taubes rotation in many-dyon configurations

Finally, it is interesting to analyse the relative orientation of the dyons in color space. In Section 2 we have described how the Taubes winding in a DD caloron could be detected in a gauge independent way. The analysis is also here, for real cooled configurations, simplified by the observation that at the center of a dyon both electric E_i^a and magnetic B_i^a field strengths (which satisfy (anti) self-duality $E_i^a = \pm B_i^a$) form orthogonal matrices in color (a) and space (i) indices. Thus, it suffices to consider three ($i = 1, 2, 3$) vectors in color space $E_i^a(\vec{x})$ forming a local reference frame at the center of a dyon with which any other local reference frame can be compared. The comparison can be made in a gauge invariant manner by connecting the centers at which the field strengths are measured by a parallel transporter, the Schwinger line.

The exploration of a few of semi-classical lattice configurations containing superpositions of several D and \bar{D} has shown the following common features. All dyons with negative peak value of the Polyakov loop have more or less random color orientation relative to each other, but this relative orientation is static along the time axis. For dyons with a positive peak value of the Polyakov loop holds the same. Also their orientation relative to each other seems to be random but static. But the relative orientation between the $L = +1$ and the $L = -1$ dyons is changing along the Euclidean time and the change is nothing but a homogeneous rotation in color space with the angle period 2π . In the analytic solution representing just two dyons (or two antidyons) this rotation is also present. It has been discussed and related to Taubes winding in Sect. 2.

To illustrate this observation let us consider a configuration obtained on the lattice of size $16^3 \times 4$ with f.h.b.c. after 400 cooling steps. The configuration contains three D and one \bar{D} as shown in Table 2. We have taken the first D as the reference point with

Table 2: Configuration of 3 D and 1 \bar{D} , obtained after 400 cooling steps with f.h.b.c. from an equilibrium configuration produced at $\beta = 2.2$ on a $16^3 \times 4$ lattice.

Type	3D position	Polyakov loop
D	$\vec{x}_1 = (5, 3, 2)$	-1
D	$\vec{x}_2 = (12, 6, 3)$	-1
D	$\vec{x}_3 = (13, 14, 5)$	+1
\bar{D}	$\vec{x}_4 = (5, 7, 13)$	-1

respect to which the relative color orientations of the other dyons and the antidyon were determined. We have calculated the matrices (cf. eq. (13)) $R_{ik}^{12}(t)$, $R_{ik}^{13}(t)$ and $R_{ik}^{14}(t)$. They show the relative orientations of the objects $n = 2, 3, 4$ – represented by their electric fields $E_k(\vec{x}_n, t) = E_k^a(\vec{x}_n) \frac{\tau^a}{2}$ which appear parallel transported to the position of the first object in the form $\mathcal{S}(\vec{x}_1, t; \vec{x}_n, t) E_k(\vec{x}_n, t) \mathcal{S}^+(\vec{x}_1, t; \vec{x}_n, t)$ – with respect to the first object – represented by its electric fields $E_k(\vec{x}_1)$. Then the evolution in time of the relative orientation can be investigated. While the matrices $R_{ik}^{12}(t) = \text{tr}(E_i(\vec{x}_1, t) \mathcal{S} E_k(\vec{x}_2, t) \mathcal{S}^+)$,

and $R_{ik}^{14}(t)$ turned out to be constant in time, the matrix $R_{ik}^{13}(t)$ performed a color rotation with a constant angle increment $\pi/2$ from one time slice to the next time slice about the color axis $\vec{n} = (-0.919, 0.278, 0.275)$. The orientation of this axis seems to be random, but the rotation angle is well-defined. For $N_t = 4$ it corresponds to a full color rotation over the full Euclidean time period. Our general observation illustrated by this example of a moderately complicated superposition shows that also these more complicated objects exhibit a strong correlation in the color orientation analogous to that present in a single DD KvB pair. A semi-classical approximation of the path integral would have to take into account this kind of color correlation.

6 Conclusions

We have generated $SU(2)$ lattice gauge fields at non-zero temperature in the confinement phase. We have cooled them in order to analyse their topological content. Fixed holonomy spatial boundary conditions have been used as well as standard periodic boundary conditions. The results for these two kinds of boundary conditions semi-quantitatively agree with each other. This is specific for ensembles describing the confinement phase.

Independently of the boundary conditions we have found superpositions of calorons, dyons and antidyons, the latter with positive and negative non-integer topological charges. The topological lumps appear also as peaks of the Polyakov loop modulus $|L(\vec{x})|$, with calorons being a limiting case with a close pair of $L(\vec{x}) = \pm 1$. Investigating also the localization behavior of the real eigenvalue modes of the (non-Hermitian) Wilson-Dirac operator we could present convincing evidence that for calorons and for dyon-dyon pairs an interpretation in terms of KvB solutions is natural. Choosing time-periodic and time-antiperiodic boundary conditions for the fermions focusses on $L(\vec{x}) = -1$ or $L(\vec{x}) = 1$ dyons, respectively.

On higher action plateaus we have found that the dynamics generically leads to non-trivial holonomy outside the lumps of action and topological charge. The multi-dyon-antidyon structure can be finally resolved by a combination of two tools: localization of fermionic real modes and the relative color-orientation of the color-electric field strength.

A semi-classical treatment of the path integral at non-zero temperature close to the deconfinement phase transition should be built on superpositions of calorons, dyons and antidyons, however with the holonomy as a free parameter.

We have seen that such superpositions would imply a strong correlation in the relative color orientation (and its Euclidean time dependence) between pairs of seemingly independent topological lumps. To the best of our knowledge, such superpositions have not yet been constructed analytically.

It is already clear that the development of a semi-classical approach based on solutions with non-trivial holonomy is much more complicated than the instanton (caloron) gas or liquid, and it might turn out not to lead to a practicable model.

Nevertheless, facing the non-trivial structures found in this paper might contribute to a better understanding of the mechanism driving the deconfinement transition. In as

far a certain working picture of a dilute gas of these configurations can be developed and whether it will improve our understanding of quark confinement itself remains an open question to which we hope to come back in the next future.

Acknowledgments

We are grateful to P. van Baal and Z. Fodor for discussions and useful comments. One of us (S.S.) acknowledges computational assistance by F. Hofheinz. E.-M. I. gratefully appreciates the support by the Ministry of Education, Culture and Science of Japan (Monbu-Kagaku-sho) and thanks H. Toki for the hospitality at RCNP.

This work was partly supported by RFBR grants 02-02-17308 and 01-02-17456, by the INTAS grant 00-00111 and the CRDF award RP1-2364-MO-02.

References

- [1] Y. Nambu, Phys. Rev. **D10** (1974) 4262;
G. 't Hooft, in: "High Energy Physics", EPS International Conference, Palermo 1975, A. Zichichi (Ed.); S. Mandelstam, Phys. Rept. **23 C** (1976) 245.
- [2] T. A. DeGrand and D. Toussaint, Phys. Rev. **D22** (1980) 2478.
- [3] A. S. Kronfeld, M. L. Laursen, G. Schierholz, and U.-J. Wiese, Phys. Lett. **B198** (1987) 516; and see e.g. H. Shiba and T. Suzuki, Phys. Lett. **B333** (1994) 461;
G. S. Bali, V. Bornyakov, M. Müller-Preussker, and K. Schilling, Phys. Rev. **D54** (1996) 2863; V. Bornyakov, et al., Nucl. Phys. Proc. Suppl. **106&107** (2002) 634.
- [4] G. 't Hooft, Nucl. Phys. **B190** (1981) 455.
- [5] A. Di Giacomo, B. Lucini, L. Montesi, and G. Paffuti, Nucl. Phys. Proc. Suppl. **74** (1999) 405; Phys. Rev. **D61** (2000) 034503,034504.
- [6] T. Suzuki, Prog. Theor. Phys. **80** (1988) 929;
S. Maedan and T. Suzuki, Prog. Theor. Phys. **81** (1989) 229.
- [7] H. Suganuma, S. Sasaki, and H. Toki, Nucl. Phys. **B435** (1995) 207;
S. Sasaki, H. Suganuma, and H. Toki, Prog. Theor. Phys. **94** (1995) 373.
- [8] T. Suzuki et al., Nucl. Phys. Proc. Suppl. **83** (2000) 550; S. Fujimoto, S. Kato, T. Suzuki, and T. Tsunemi, Prog. Theor. Phys. Suppl. **138** (2000) 36.
- [9] J. M. Carmona, M. D'Elia, A. Di Giacomo, B. Lucini, and G. Paffuti, Phys. Rev. **D64** (2001) 114507.
- [10] C. G. Callan, R. F. Dashen, and D. J. Gross, Phys. Rev. **D17** (1978) 2717.

- [11] E.-M. Ilgenfritz and M. Müller-Preussker, Nucl. Phys. **B184** (1881) 443.
- [12] E. V. Shuryak, Nucl. Phys. **B203** (1982) 93,116,140;
E. V. Shuryak, Phys. Rept. **115** (1984) 151;
E. V. Shuryak, Nucl. Phys. **B302** (1988) 559,574,599,621.
- [13] D. Dyakonov and V. Petrov, Nucl. Phys. **B245** (1984) 259.
- [14] E. V. Shuryak and J. L. Rosner, Phys. Lett. **B218** (1989) 72.
- [15] A. A. Belavin, A. M. Polyakov, A. S. Schwartz, and Yu. S. Tyupkin, Phys. Lett. **B59** (1975) 85.
- [16] see the review: T. Schäfer and E. V. Shuryak, Rev. Mod. Phys. **70** (1998) 323.
- [17] M. Fukushima, H. Suganuma, A. Tanaka, H. Toki, and S. Sasaki,
Nucl. Phys. Proc. Suppl. **63** (1998) 513.
- [18] M. Fukushima, E.-M. Ilgenfritz, and H. Toki, Phys. Rev. **D64** (2001) 034503.
- [19] M. N. Chernodub and F. V. Gubarev, JETP Letters **62** (1995) 100, e-Print Archive:
hep-th/9506026.
- [20] V. Bornyakov and G. Schierholz, Phys. Lett. **B384** (1996) 190.
- [21] H. Markum, W. Sakuler, and S. Thurner, Nucl. Phys. Proc. Suppl. **47** (1996) 254;
M. Feurstein, H. Markum, and S. Thurner, Phys. Lett. **B396** (1997) 203.
- [22] M. Feurstein, E.-M. Ilgenfritz, M. Müller-Preussker, and S. Thurner, Nucl.
Phys. **B511** (1998) 421; E.-M. Ilgenfritz, H. Markum, M. Müller-Preussker, and
S. Thurner, Phys. Rev. **D58** (1998) 094502.
- [23] M. Fukushima, H. Suganuma, and H. Toki, Phys. Rev. **D60** (1999) 094504.
- [24] For very recent reviews all presented at the *NATO Advanced Research Workshop
on Confinement, Topology, and other Nonperturbative Aspects of QCD*, Stara Lesna,
Slovakia, January 2002 and references therein see
M. Faber, J. Greensite, and S. Olejnik, e-Print Archive: hep-lat/0204020; H. Rein-
hardt, e-Print Archive: hep-th/0204194; M. Engelhardt, e-Print Archive: hep-
lat/0204021.
- [25] A. Montero and J. W. Negele, Phys. Lett. **B533** (2002) 322.
- [26] D. J. Gross, R. D. Pisarski, and L. G. Yaffe, Rev. Mod. Phys. **53** (1981) 43.
- [27] B. J. Harrington and H. K. Shepard, Phys. Rev. **D17** (1978) 2122; Phys. Rev. **D18**
(1978) 2990.
- [28] T. C. Kraan and P. van Baal, Phys. Lett. **B435** (1998) 389.

- [29] T. C. Kraan and P. van Baal, Nucl. Phys. **B533** (1998) 627.
- [30] M. K. Prasad and C. M. Sommerfield, Phys. Rev. Lett. **35** (1975) 760;
E. B. Bogomol'nyi, Sov. J. Nucl. Phys. **24** (1976) 449.
- [31] M. García Pérez, A. González-Arroyo, A. Montero, and P. van Baal,
JHEP **06** (1999) 001; e-Print Archive: hep-lat/9903022.
- [32] E.-M. Ilgenfritz, M. L. Laursen, M. Müller-Preussker, G. Schierholz, and H. Schiller,
Nucl. Phys. **B268** (1986) 693.
- [33] E.-M. Ilgenfritz, M. Müller-Preussker, and A. I. Veselov, Proceedings NATO Ad-
vanced Workshop *Lattice Fermions and Structure of the Vacuum*, Dubna, 1999; e-Print
Archive: hep-lat/0003025.
- [34] E.-M. Ilgenfritz, B. Martemyanov, M. Müller-Preussker, and A. I. Veselov, Nucl.
Phys. Proc. Suppl. **94** (2001) 407.
- [35] E.-M. Ilgenfritz, B. Martemyanov, M. Müller-Preussker, and A. I. Veselov, Nucl.
Phys. Proc. Suppl. **106&107** (2002) 589.
- [36] M. N. Chernodub, T. C. Kraan, and P. van Baal, Nucl. Phys. Proc. Suppl. **83** (2000)
556.
- [37] M. L. Laursen and G. Schierholz, Z. Phys. **C38** (1988) 501.
- [38] G. t'Hooft, Phys. Rev. **D14** (1976) 3432; Erratum Phys. Rev. **D18** (1978) 2199.
- [39] C. Taubes, Comm. Math. Phys. **86** (1982) 257,299.
- [40] M. García Pérez, A. González-Arroyo, C. Pena, and P. van Baal,
Phys. Rev. **D60** (1999) 031901.
- [41] J. Engels, J. Fingberg, and V. K. Mitrjushkin, Phys. Lett. **B298** (1993) 154;
J. Engels, S. Mashkevich, T. Scheideler, and G. Zinovev, Phys. Lett. **B365** (1996)
219.
- [42] H. Neff, N. Eicker, T. Lippert, J. W. Negele, and K. Schilling,
Phys. Rev. **D64** (2001) 114509.
- [43] see: <http://www.caam.rice.edu/software/ARPACK/>.

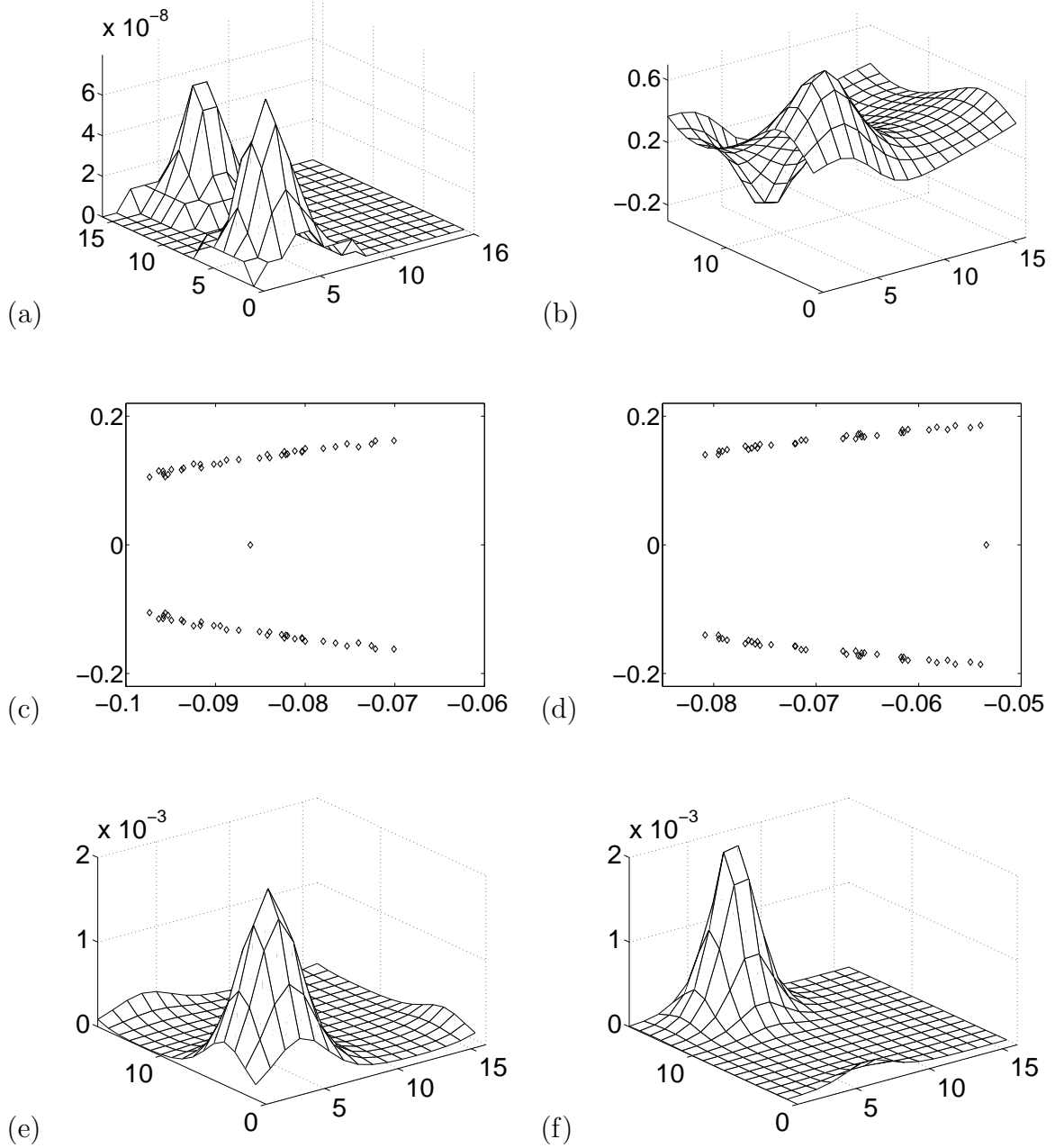


Figure 1: Various portraits of a selfdual DD pair obtained by cooling under periodic gluonic boundary conditions. The sub-panels show: appropriate $2D$ cuts of the topological charge density (a) and of the Polyakov loop (b), the plot of lowest fermionic eigenvalues (c,d) and the $2D$ cut of the real-mode fermion densities (e,f), for the cases of time-periodic (c,e) and time-antiperiodic (d,f) fermionic boundary conditions, respectively ($\beta = 2.2$ and lattice size $16^3 \times 4$).

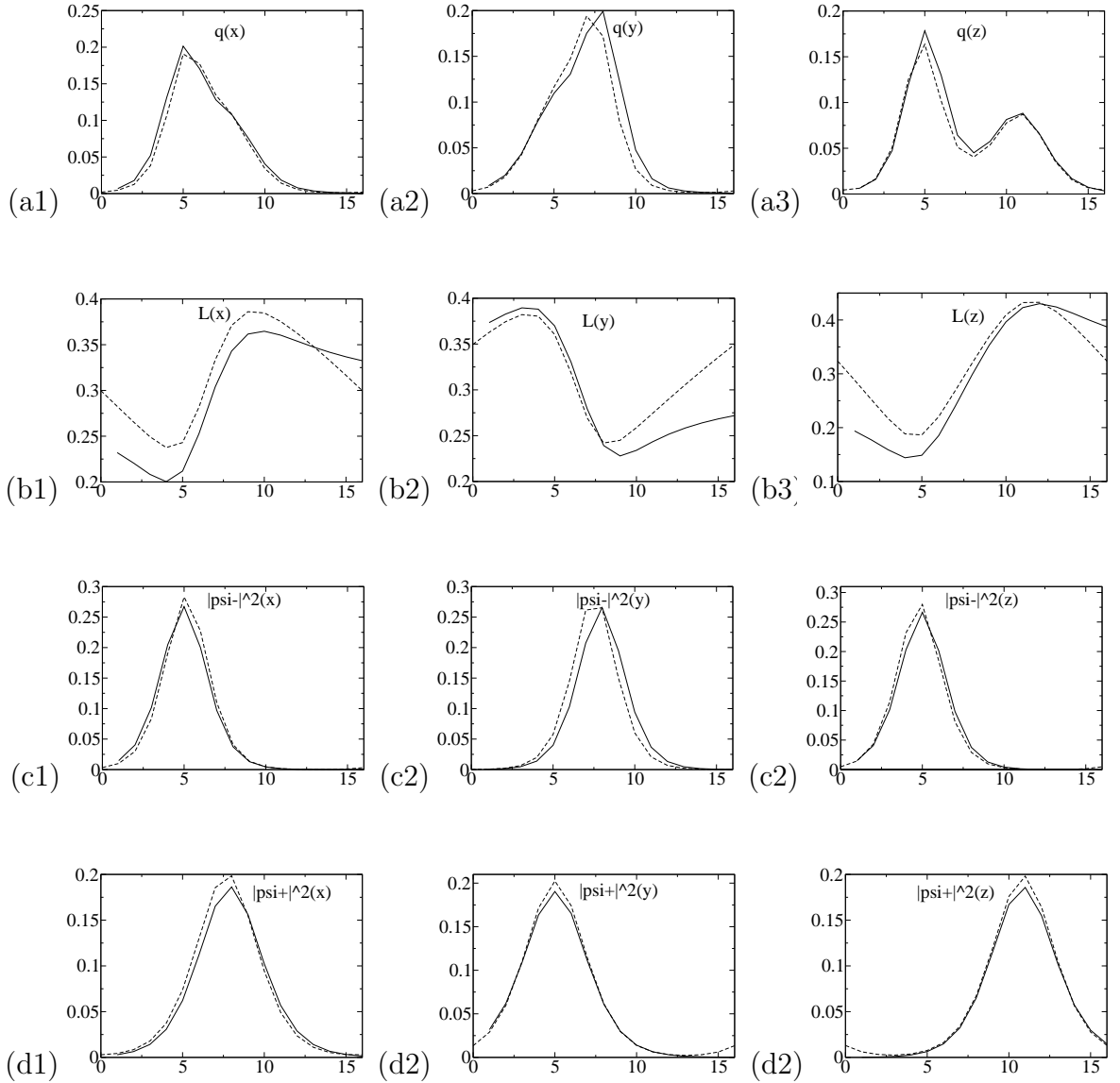


Figure 2: The DD lattice configuration of Fig. 1 (dashed lines), fitted by the KvB solution (solid lines) according to the action density, shown in three spatial views ($1D$ projections). In (a1),(a2),(a3) the topological charge density is summed over the two unspecified spatial coordinates. In (b1),(b2),(b3) the Polyakov loop is averaged over the two unspecified spatial coordinates. In the time-antiperiodic case (c1,c2,c3) or the time-periodic case (d1,d2,d3), respectively, the fermion density it is summed over the two unspecified spatial coordinates.

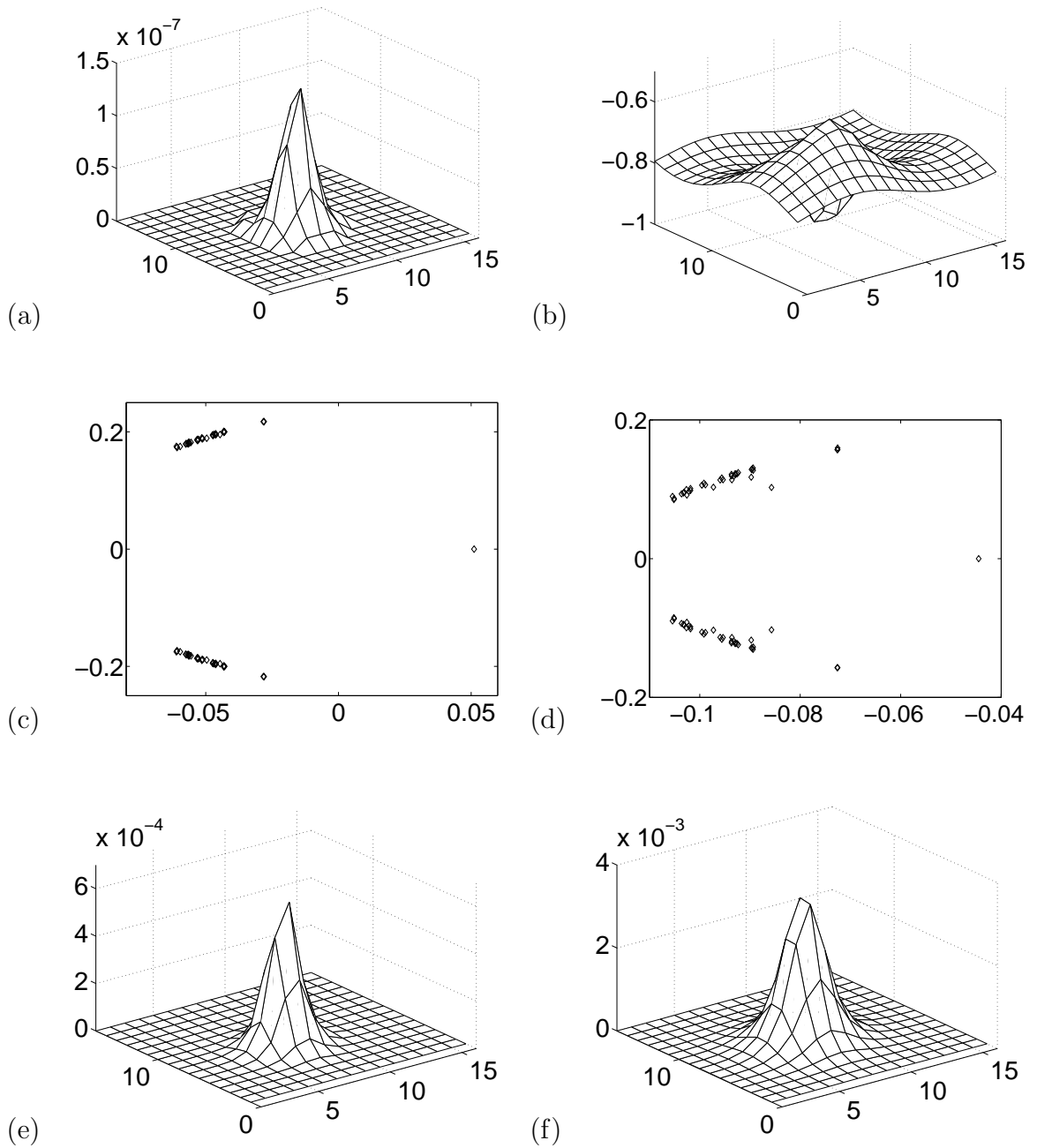


Figure 3: Various portraits of a selfdual *CAL* configuration obtained by cooling under periodic gluonic boundary conditions. The sub-panels show: appropriate 2D cuts of the topological charge density (a) and of the Polyakov loop (b), the plot of lowest fermionic eigenvalues (c,d) and the 2D cut of the real-mode fermion densities (e,f), for the cases of time-periodic (c,e) and time-antiperiodic (d,f) fermionic boundary conditions, respectively ($\beta = 2.2$ and lattice size $16^3 \times 4$).

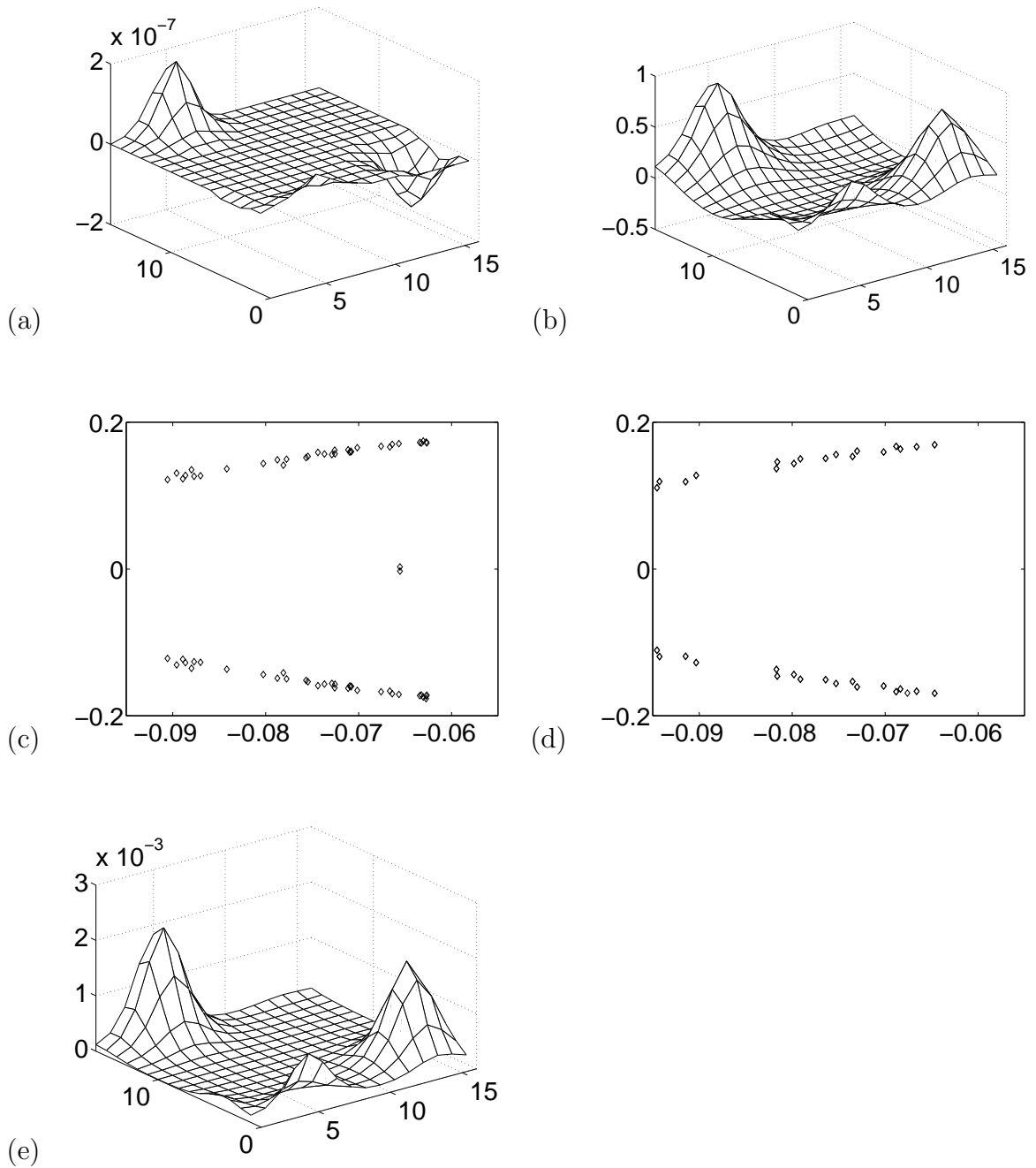


Figure 4: Various portraits of a mixed-duality $D\bar{D}$ pair obtained by cooling under periodic gluonic boundary conditions. The sub-panels show: appropriate $2D$ cuts of the topological charge density (a) and of the Polyakov loop (b), the plot of lowest fermionic eigenvalues (c,d) for the cases of time-periodic (c) and time-antiperiodic (d) fermionic boundary conditions, respectively ($\beta = 2.2$ and lattice size $16^3 \times 4$). A $2D$ cut of the fermionic mode density related to the two distinct *almost* real eigenvalues in (c) is shown in (e).

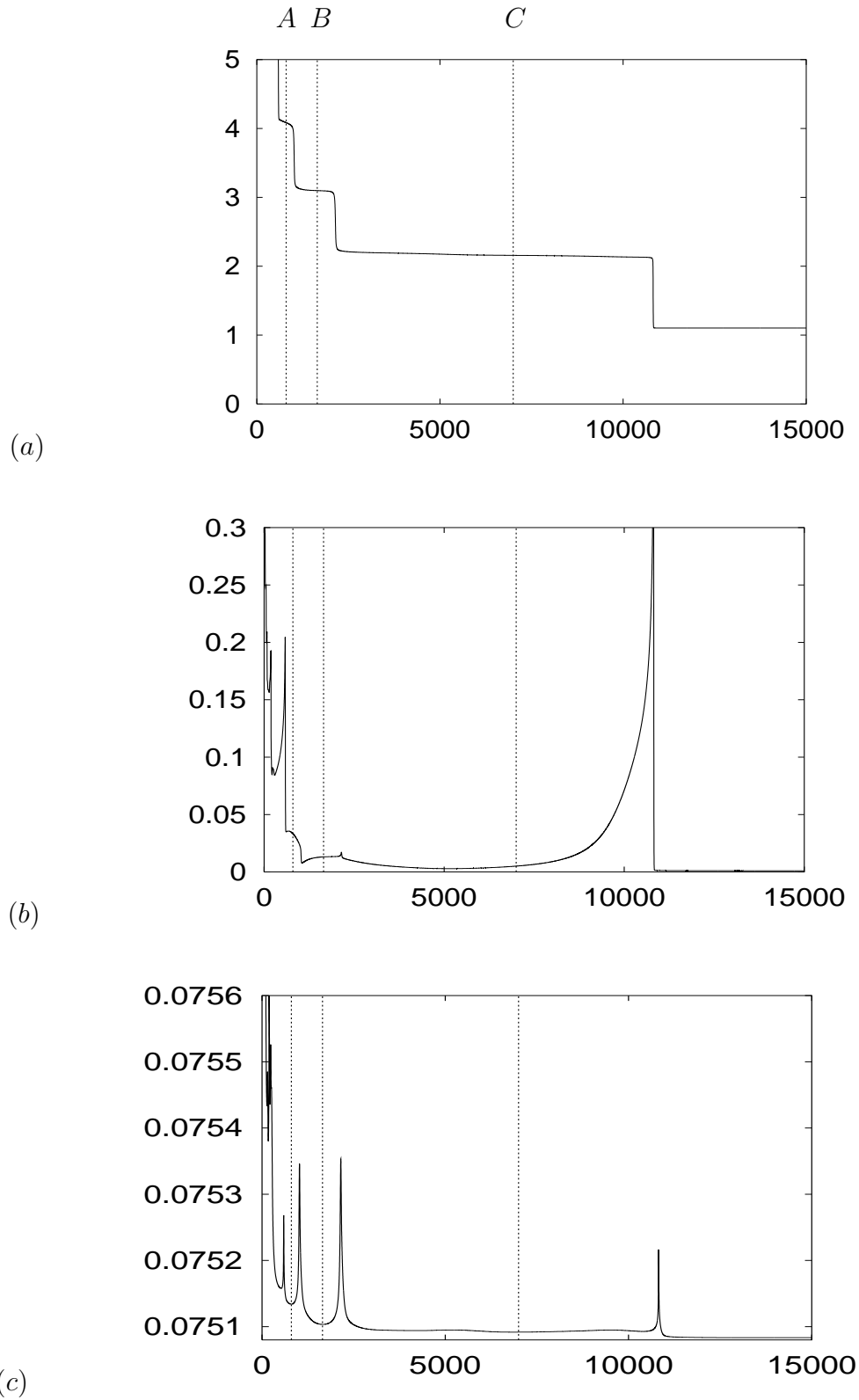
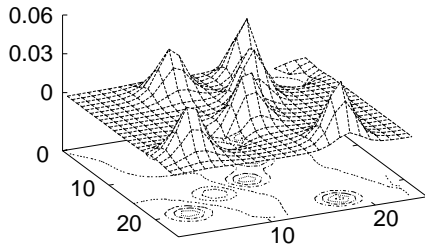
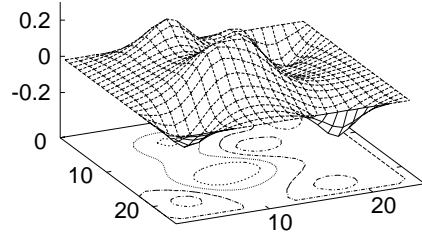


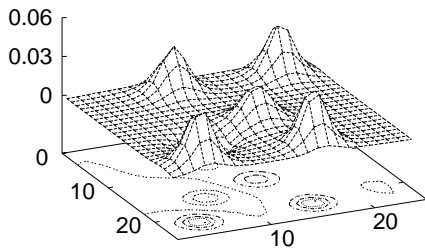
Figure 5: Part of the cooling history for a gauge field configuration taken from the Monte Carlo sample generated at $\beta = 2.2$ on a $24^3 \times 4$ lattice, with f.h.b.c. of $L_{\vec{x} \in \Omega} = 0$. The sub-panels show: (a) full action S/S_{inst} , (b) non-stationarity δ_t and (c) mean violation Δ per link of the lattice field equations, *vs.* the number of cooling steps. The vertical dotted lines indicate the passages of Δ through local minima having occurred at 800 (A), 1650 (B) and 7000 (C) cooling steps for which the configurations will be portrayed in Figures 6, 7, 8 and 9.



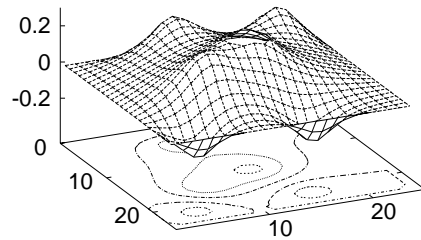
(A)



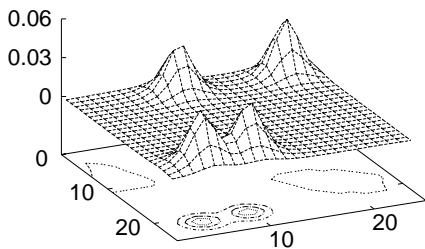
(A')



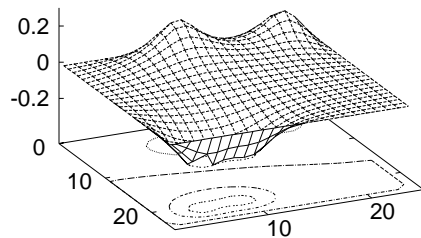
(B)



(B')



(C)



(C')

Figure 6: Configurations on the $24^3 \times 4$ lattice (from equilibrium at $\beta = 2.2$ with f.h.b.c.), as indicated in Fig. 5 after 800 (A,A'), 1650 (B,B') and 7000 (C,C') cooling steps. (A,B,C) show 2D projections of the topological charge density $q_t(x)$ and (A',B',C') of the Polyakov loop $L(\vec{x})$, respectively. Cooling has been employed with f.h.b.c., $L_{\vec{x} \in \Omega} = 0$.

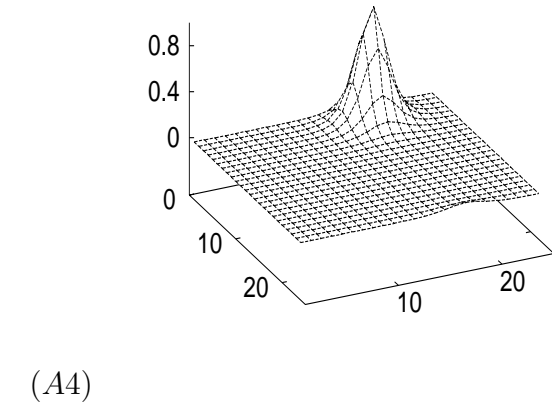
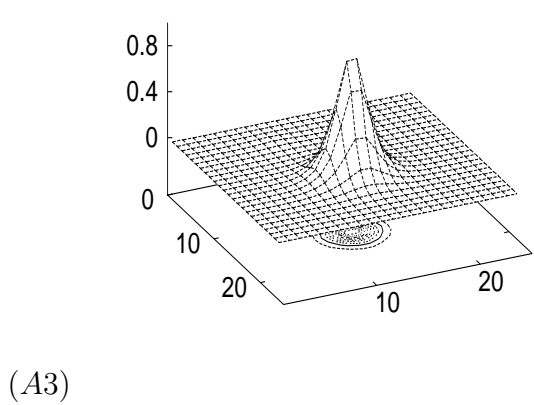
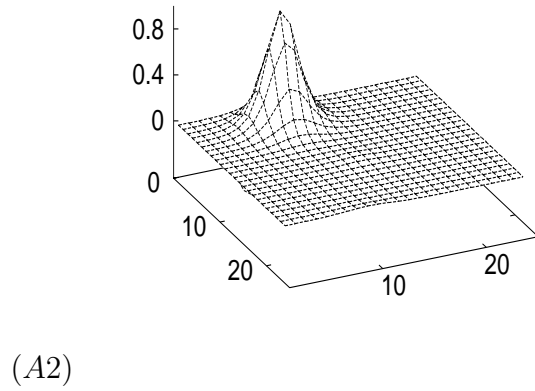
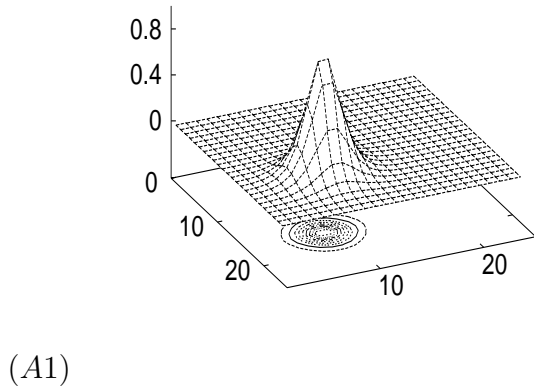
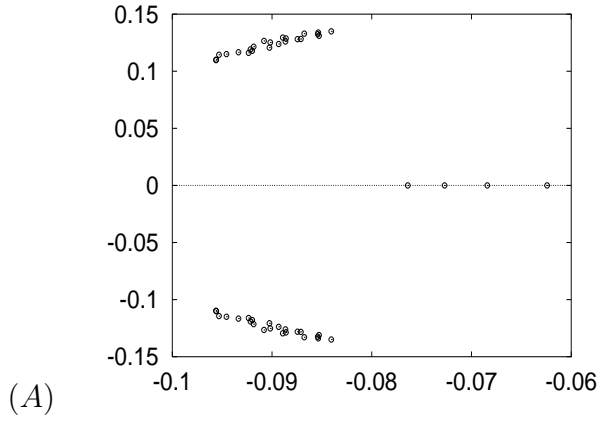


Figure 7: The lattice field configuration depicted in Fig. 6 (A,A') for 800 cooling steps (f.h.b.c.). Here (A) plots the eigenvalues of the Wilson-Dirac operator in the complex plane for $\kappa = 0.140$ and the case of time-periodic fermionic b.c.; (A1,...,A4) show 2D projections of the fermionic mode densities related to the four distinct real eigenvalues.

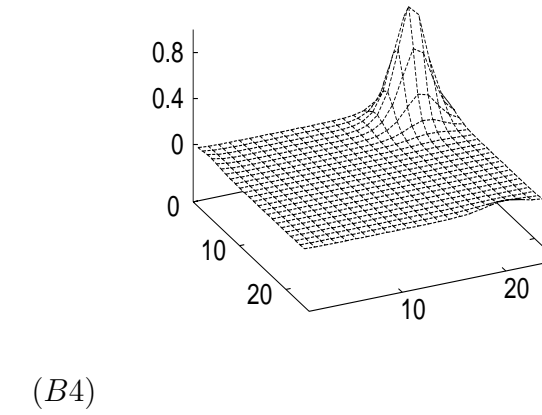
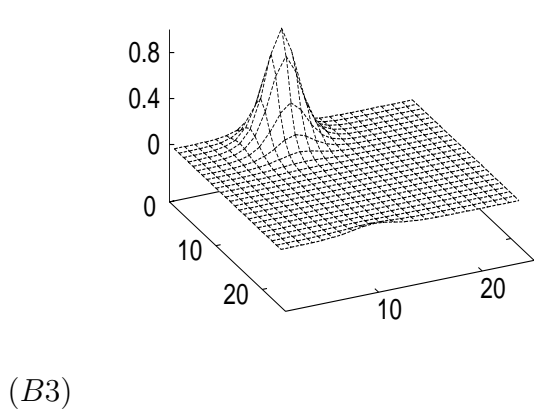
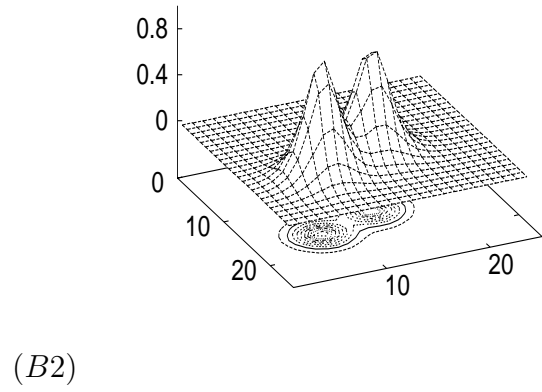
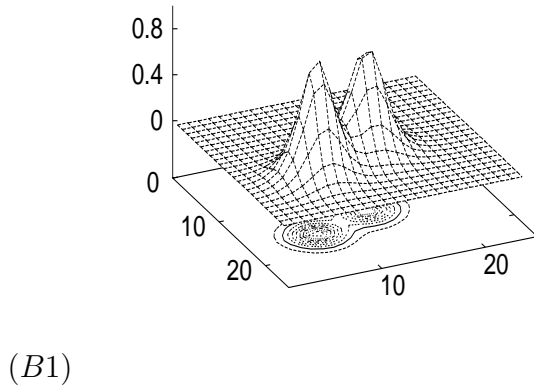
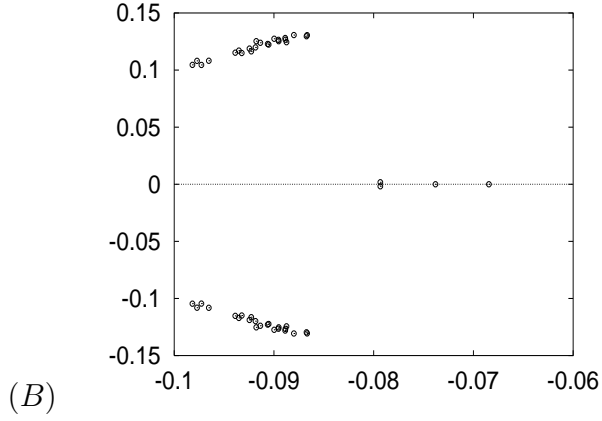


Figure 8: The lattice field configuration depicted in Fig. 6 (B,B') for 1650 cooling steps (f.h.b.c.). Here (B) plots the eigenvalues of the Wilson-Dirac operator in the complex plane for $\kappa = 0.140$ and the case of time-periodic fermionic b.c.; (B1,B2) show 2D projections of the fermionic mode densities related to the two distinct *almost* real eigenvalues, whereas (B3,B4) present the densities related to the two real eigenvalues.

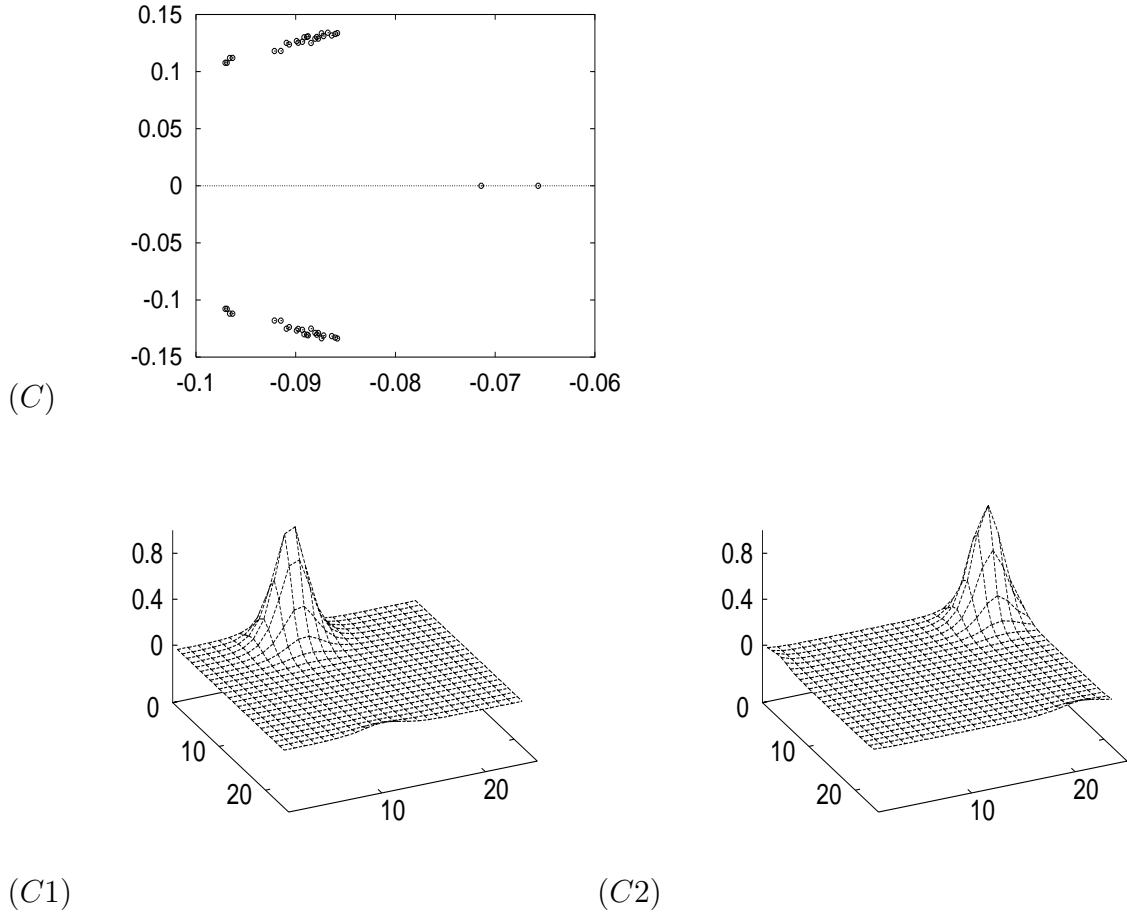


Figure 9: The lattice field configuration depicted in Fig. 6 (C,C') for 7000 cooling steps (f.h.b.c.). Here (C) plots the eigenvalues of the Wilson-Dirac operator in the complex plane for $\kappa = 0.140$ and the case of time-periodic fermionic b.c.; (C1, C2) show $2D$ projections of the fermionic mode densities related to the two real eigenvalues.

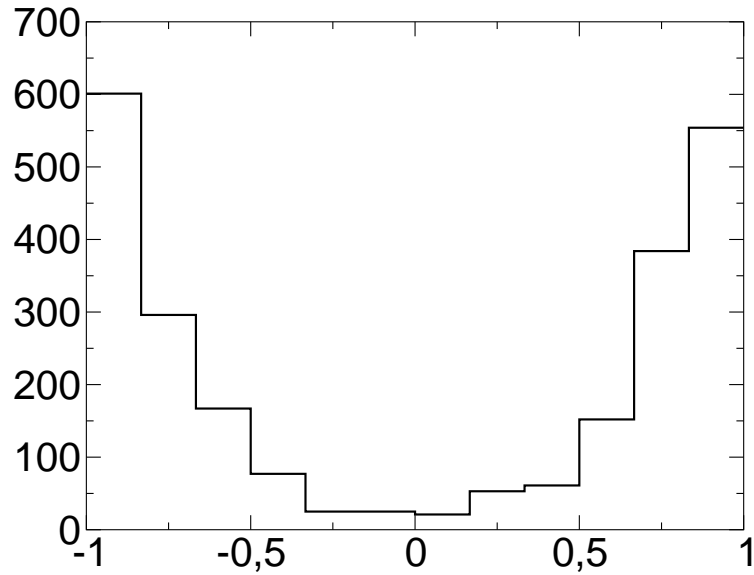


Figure 10: Histogram $P(L)$ of the values of the Polyakov loop $L(\vec{x})$ taken at \vec{x} where time-like Abelian (anti)monopoles are found. The data represent cooling plateaus at $m = 4$ obtained at $\beta = 2.2$ with lattice size $16^3 \times 4$. $O(2400)$ non-vanishing monopole charges were collected.

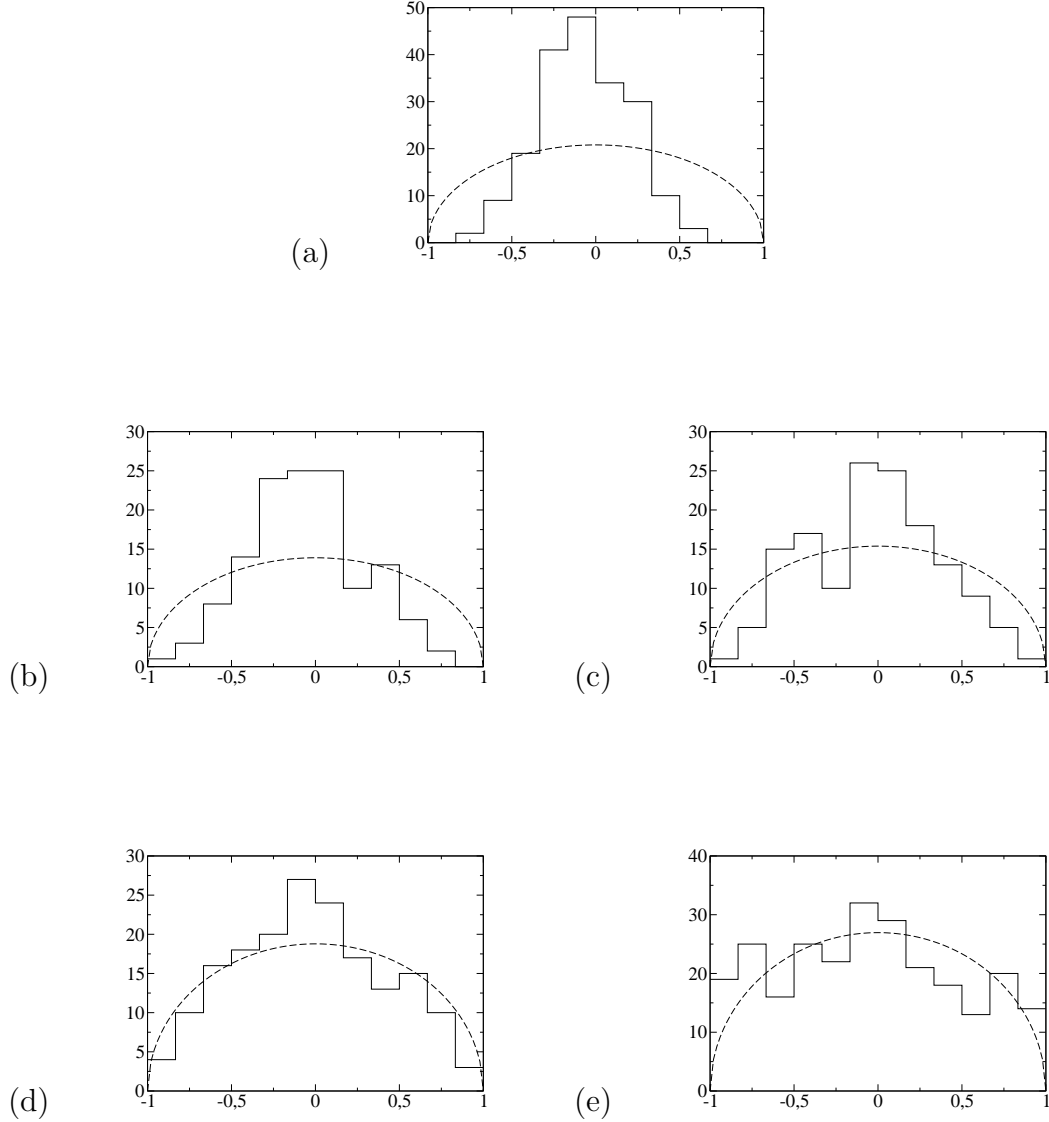


Figure 11: Histogram $P(L_\infty)$ of the values of the Polyakov loop at "infinity" (as explained in the text) seen on the first plateau (a) and at plateaus with $m \simeq 4$ (b), $m \simeq 3$ (c), $m \simeq 2$ (d), $m \simeq 1$ (e). For comparison the distribution expected from the pure Haar measure $P_{\text{Haar}}(L) \sim \sqrt{1-L^2}$ is shown with the same normalization (dashed lines). The equilibrium ensemble was generated at $\beta = 2.2$, the lattice size is $16^3 \times 4$, cooling was performed using periodic b.c., $O(200)$ configurations were investigated.

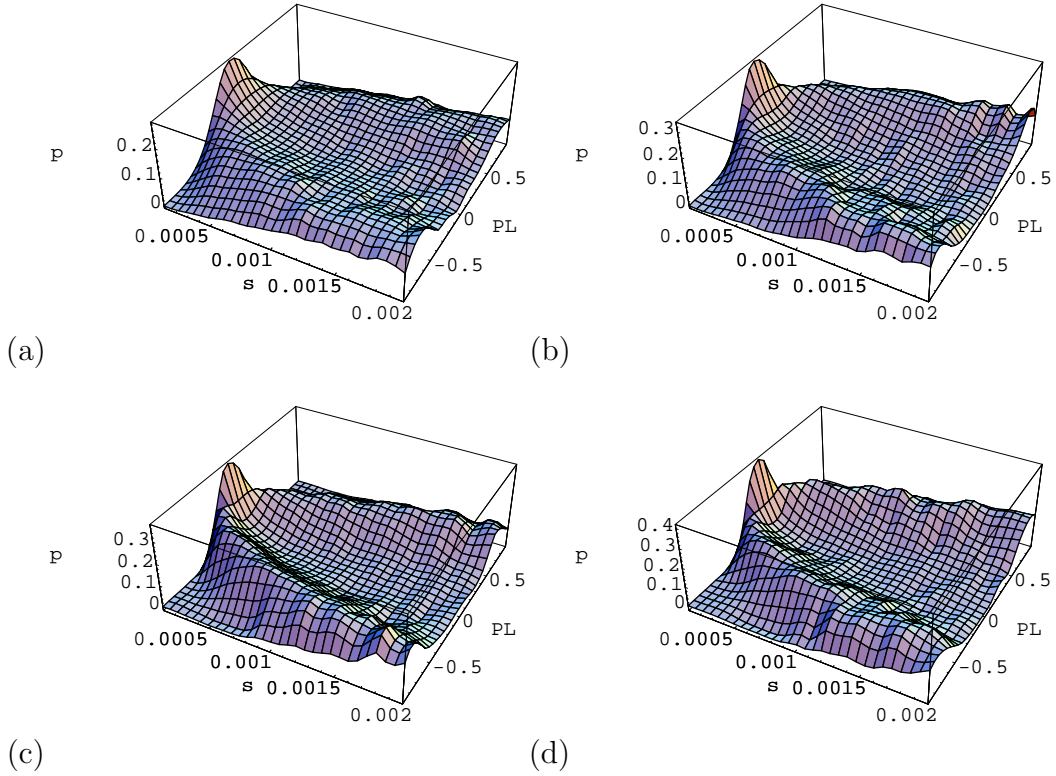


Figure 12: Conditional distributions $P[L|\zeta]$ relating local values of $L(\vec{x})$ with the spatial action density $\zeta(\vec{x})$ for cooled configurations at plateaus with $7 \geq m \geq 5$ (a), $m \simeq 4$ (b), $m \simeq 3$ (c) and $m \simeq 2$ (d). The equilibrium ensemble was generated at $\beta = 2.2$, the lattice size is $16^3 \times 4$, cooling was performed using p.b.c.

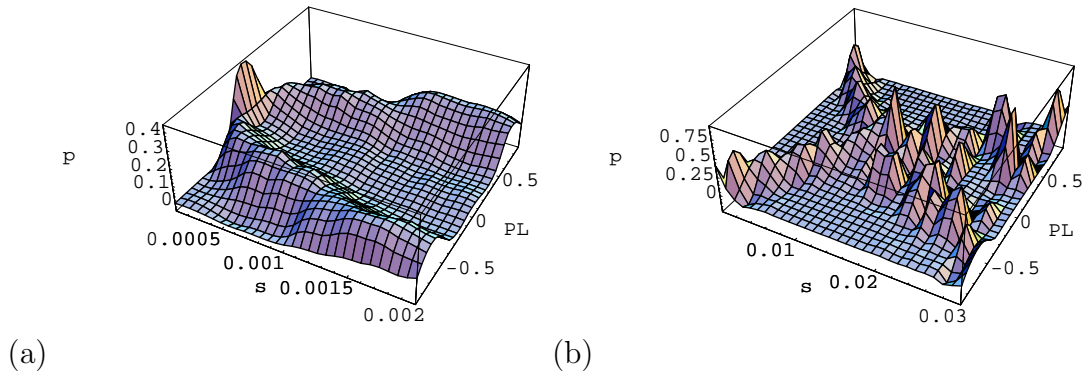


Figure 13: Conditional distributions $P[L|\zeta]$ as in Fig. 12, obtained for random KvB solutions (DD or CAL) (a) and for calorons with trivial holonomy (b), for comparison.